Basin Research

EAGE

Basin Research (2011) **23**, 571–590, doi: 10.1111/j.1365-2117.2011.00502.x

Spatial variation of erosion in a small, glaciated basin in the Teton Range, Wyoming, based on detrital apatite (U-Th)/He thermochronology

Lisa M. Tranel,*[1] James A. Spotila,* Michal J. Kowalewski* and Claire M. Waller†

**Department of Geosciences, Virginia Tech, Blacksburg, VA*

†*Division of Geological and Planetary Sciences, California Institute of Technology, Pasadena, CA*

ABSTRACT

Evolution of mountain landscapes is controlled by dynamic interactions between erosional processes that vary in efficiency over altitudinal domains. Evaluation of spatial and temporal variations of individual erosion processes can augment our understanding of factors controlling relief and geomorphic development of alpine settings. This study tests the application of detrital apatite (U-Th)/He thermochronology (AHe) to evaluate variable erosion in small, geologically complex catchments. Detrital grains from glacial and fluvial sediment in a single basin were dated and compared with a bedrock derived age-elevation relationship to estimate spatial variation in erosion over different climate conditions in the Teton Range, Wyoming. Controls and pitfalls related to apatite quality and yield were fully evaluated to assess this technique. Probability density functions comparing detrital age distributions identify variations in erosional patterns between glacial and fluvial systems and provide insight into how glacial, fluvial, and hillslope processes interact. Similar age distributions representing erosion patterns during glacial and interglacial times suggest the basin may be approaching steady-state. This also implies that glaciers are limited and no longer act as buzzsaws or produce relief. However, subtle differences in erosional efficiency do exist. The high frequency of apatite cooling ages from high altitudes represents either rapid denudation of peaks and ridges by mass wasting or an artifact of sample quality. A gap in detrital ages near the mean age, or mid-altitude, indicates the fluvial system is presently transport limited by overwhelming talus deposits. This study confirms that sediment sources can be traced in small basins with detrital AHe dating. It also demonstrates that careful consideration of mineral yield and quality is required, and uniform erosion assumptions needed to extract basin thermal history from detrital ages are not always valid.

INTRODUCTION

The character of mountain topography, including relief, is a function of uplift and variation in erosional efficiency across altitudinal domains within a drainage basin. For example, the interaction of glacial and hillslope erosion in alpine environments tends to produce deep valleys and steep ridges. Variability and efficiency of erosional agents within altitudinal domains are in turn controlled by mechanics of each process, environmental conditions, such as climate and bedrock strength, and interactions with other erosional processes (Li *et al.*, 2005; Hales & Roering, 2007). Complex interactions and feedbacks between processes make topography sensitive to changes in the aforementioned boundary conditions, which may result in transient responses in landscape evolution (Harkins *et al.*, 2007; Oskin & Burbank, 2007; Riihimaki *et al.*, 2007). To determine the controls of mountain topography and basin development, it is therefore necessary to evaluate both the nature of individual processes and their dynamic interactions.

Identifying spatial and temporal trends of erosion enables assessment of mechanisms that control topography in multiprocess catchments, including transient development of alpine settings. Relative efficiency of erosional agents is investigated with channel and hillslope gradients, profiles, and basin hypsometries (Brocklehurst & Whipple, 2004, 2007; Harkins *et al.*, 2007; Ouimet *et al.*, 2009). These studies commonly focus on basins with a single dominant process, such as glacial or fluvial incision (Harbor, 1992; Schmidt & Montgomery, 1995; Small & Anderson, 1998; Montgomery, 2002), thus avoiding the incorporation of complex, yet significant, interactions with other processes. Using topography alone is limiting, because characterization of erosional efficiency is qualitative and cumulative, whereas landscapes are functions of continuous competition between erosional agents and may be

[1] Current address: Department of Geography-Geology, Illinois State University, Campus Box 4400, Normal, IL 61790-4400, USA

Correspondence: Lisa M. Tranel, Department of Geosciences, Virginia Tech, 4044 Derring Hall (0420), Blacksburg, VA 24061, USA. E-mail: ltranel@ilstu.edu

overprinted by specific events in geomorphic history. Attempts to define temporal constraints on landscape evolution under glacial–interglacial conditions illustrate the significance of coupling between erosional processes, as individual agents alone may not effectively change relief (Kirkbride & Matthews, 1997; Whipple *et al.*, 1999; Arsenault & Meigs, 2005; Anderson *et al.*, 2006; Attal & Lave, 2006). Since few previous studies have quantified or inferred rates of different processes within individual basins (Burbank *et al.*, 1996; Korup & Schlunegger, 2007), we examine spatial and temporal erosion patterns in a basin of mixed glacial and fluvial history using detrital thermochronology.

Detrital thermochronology is a powerful tool that has evolved over the past few decades to provide a window into exhumation history, thermal structure, and basin evolution. These techniques applied to lithified and modern sediment have proven useful for determining provenance, tectonic or geomorphic histories, and denudation rates of basins (Cerveny *et al.*, 1988; Corrigan & Crowley, 1992; Garver *et al.*, 1999; Fedo *et al.*, 2003; Cawood *et al.*, 2007). Detrital grains are also used as tracers to understand variable erosion rates and relief development (Brewer *et al.*, 2003; Carrapa & Strecker, 2005; Rahl *et al.*, 2007). Pioneering work recently used modern detrital sediments to study spatial erosion variability and paloerelief in tectonically active mountains and glacial and fluvial basins (Stock & Montgomery, 1996; Ruhl & Hodges, 2005; Stock *et al.*, 2006; Vermeesch, 2007). The inherent advantage is that information about an entire basin can be obtained from a single 'grab bag' of sediment (Cerveny *et al.*, 1988; Brewer *et al.*, 2003; Cawood *et al.*, 2003; Fedo *et al.*, 2003; Rahl *et al.*, 2003). Since detrital thermochronology may potentially constrain rates of different erosional processes through time, we apply this technique to investigate coupling of erosional agents in a single alpine basin.

The purpose of this study is to test a technique that could potentially quantify variations of erosion where dominant erosional processes are not easily defined. We investigate the distinctive topography of the Teton Range, which was shaped by tectonics, climate, and interactions between glacial, fluvial, and mass wasting processes (Roberts & Burbank, 1993; Love *et al.*, 2003; Foster *et al.*, 2008, 2010), making this an ideal location to study dynamic coupling of erosional agents. We use detrital apatite (U-Th)/He thermochronology (AHe) to estimate the efficiency of erosional processes acting at different altitudes and varying over short-term climatic fluctuations recorded in glacial and fluvial sediments (Ehlers & Farley, 2003; Stock *et al.*, 2006). Along with its application to studying spatial and temporal patterns of erosion, we also explore controls and pitfalls of this technique.

BACKGROUND

The Teton Range is located in northwest Wyoming (Fig. 1), and while relatively small (70 km by 25 km), is well known for its striking geomorphic expression; rugged peaks separated by deep glacial valleys, and saw tooth-like topographic profile (Fig. 2). It lies within the arcuate region of dynamic topography and active seismicity surrounding the head of the Yellowstone hotspot (Anders & Sleep, 1992; Pierce & Morgan, 1992; Hampel *et al.*, 2007).

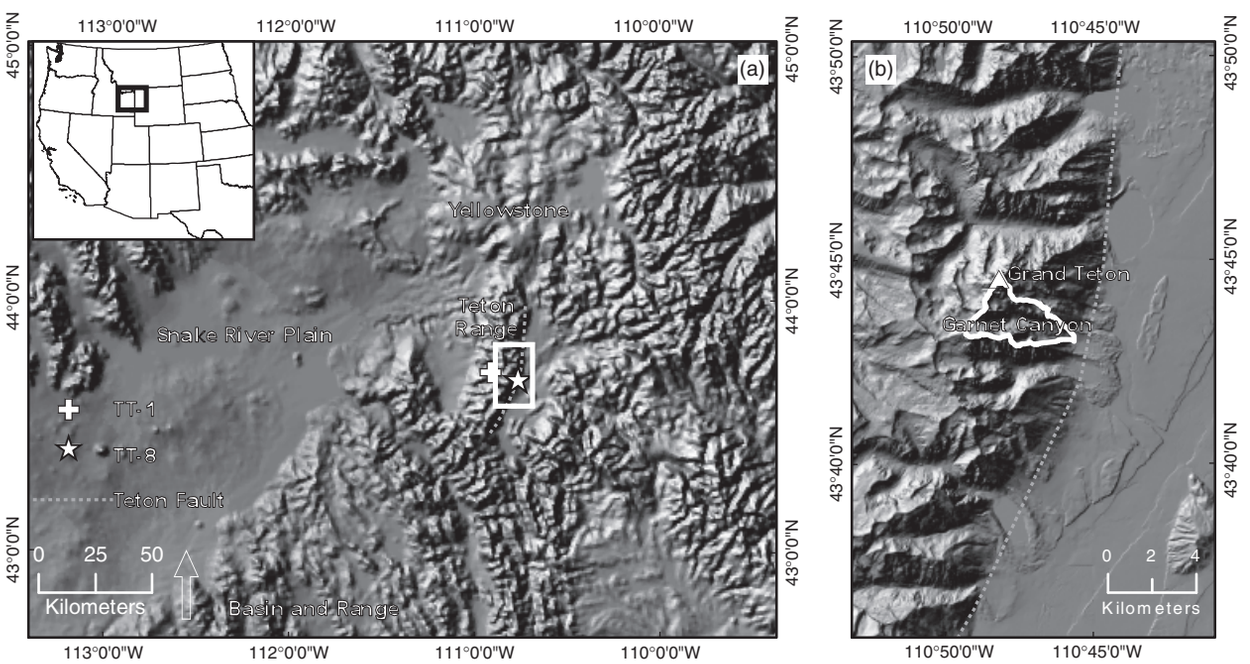

Fig. 1. Location of the Teton Range and Garnet Canyon. (a) USGS shaded relief map of the region surrounding the Teton Range. Sample TT-8 (star) is positioned near the mouth of Garnet Canyon. The location of sample TT-1 (cross) is below the unconformity on the west side of the range. The white box contains the central area of the range and canyons in this study. (b) Garnet Canyon study area. The Grand Teton is marked with a triangle.

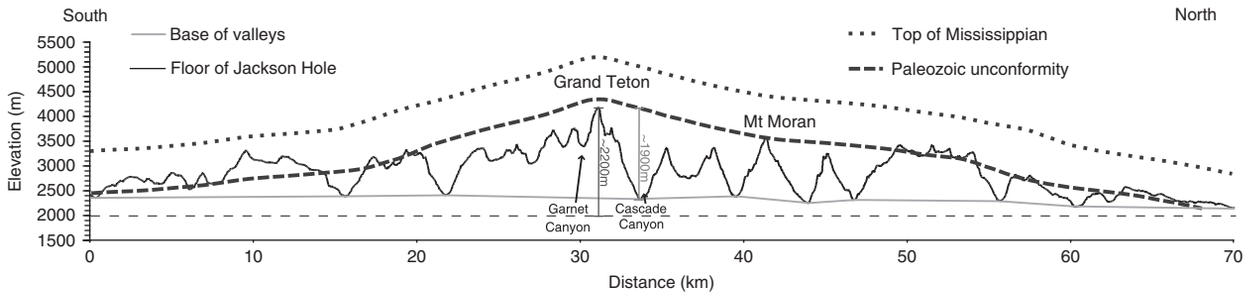

Fig. 2. Along-strike topographic profile of the Teton Range. The solid line connects high ridges across the front of the range. Note that steep walls and ridges are adjacent to deeply incised valleys, and the highest peaks are located in the central area of the range. Dashed lines indicate upper and lower boundaries of Cambrian to Mississippian sedimentary rocks that possibly existed above the Precambrian basement before onset of Neogene uplift based on the average thickness of the sedimentary section and unconformity (Love *et al.*, 2003). Peaks have not eroded much more than ~100 m below the projected Precambrian–Paleozoic unconformity, whereas the valleys have been deeply incised (Brown, 2010).

Neogene Basin and Range extension has caused uplift of the Teton Range, which initiated 9 ± 4 Ma (Love, 1977; Barnosky, 1984; Roberts & Burbank, 1993; Smith *et al.*, 1993; Leopold *et al.*, 2007) but has accelerated in the past 2–5 Ma due to arrival of the hotspot (Love *et al.*, 2003). Slip-rates on the Teton normal fault vary between 0.1–5.0 mm yr^{-1}, depending on observed time frame, location along strike, and methodology, but likely average ~1 mm yr^{-1} (Roberts & Burbank, 1993; Byrd, 1995; Machette *et al.*, 2001; Love *et al.*, 2003; Puskas & Smith, 2009). Between 50% and 80% of offset is accommodated by subsidence in the Jackson Hole Basin, with the remainder producing the Teton Range. Total structural offset is estimated at 6–9 km, with 2.5–3.5 km of displacement in the past 2 Ma (Smith *et al.*, 1993; Byrd, 1995).

Our study area in the center of the range consists of Archaean metamorphic gneiss and plutonic quartz monzonite (Bradley, 1956; Reed & Zartman, 1973; Byrd, 1995; Love *et al.*, 2003). The Mount Owen quartz monzonite, also described as muscovite and garnet bearing leucogranite, is heterogeneous due to xenoliths of layered gneiss and migmatite and dikes of aplite and pegmatite (Fig. 3) (Love *et al.*, 1992). Gneiss largely overlies monzonite and consists of interlayered amphibolite, quartzofeldspathic gneiss and schist (Reed & Zartman, 1973; Zartman & Reed, 1998; Love *et al.*, 2003; Frost *et al.*, 2006). A cap of Paleozoic strata unconformably overlies the northern, southern, and western flanks. Cambrian to Mississippian sedimentary rocks in the region reach thicknesses of ~900 m and may have once covered the central region of the range (Love *et al.*, 2003). Three-dimensional geometry of the Paleozoic unconformity shows a domal pattern of rock uplift related to Neogene normal faulting and Cretaceous-Early Tertiary Laramide folding (Roberts & Burbank, 1993; Love *et al.*, 2003; Brown, 2010). The unconformity projects a short distance above the highest peak (Grand Teton, 4198 m), and is preserved on Mount Moran (Fig. 2) (Love *et al.*, 2003; Brown, 2010). Relief between Grand Teton and the floor of nearby Cascade Canyon is ~1900 m compared with only 100 m between Grand Teton and the projected unconformity, therefore long-term valley incision has been much faster than ridge erosion.

The Teton Range is an asymmetric, west-tilted block, with the highest peaks positioned near the eastern edge of the range rather than at the drainage divide, ~4 km to the west. The tapered along strike profile is a bell-shaped curve formed by variation in slip rate along the Teton fault (Fig. 2) (Smith *et al.*, 1993; Foster *et al.*, 2010). High, isolated peaks and ridges are bordered by near vertical cliffs, scoured bedrock slopes and massive talus deposits. Cirques line the eastern drainage divide and heads of U-shaped glacial valleys (Figs 1 and 4). The range was repeatedly glaciated throughout the past 1 Ma, most recently during the Pinedale glaciation (14–44 ka, last glacial maximum or LGM), when valley glaciers reached Jackson Hole and deposited terminal moraines ~1–2 km from the base of the range (Fig. 4) (Licciardi & Pierce, 2008). Melting modern glaciers are small and exist only in cirques at high elevations where annual precipitation is highest, ranging between 40 and 200 cm yr^{-1} (Porter *et al.*, 1983; Foster *et al.*, 2010).

Recent studies examined how glacial erosion interacts with evolving topography to shape the complex Teton landscape. Foster *et al.* (2008) examined whether a 'glacial buzzsaw' (Brozovic *et al.*, 1997; Mitchell & Montgomery, 2006) controls topography in alpine settings with relatively small valley glaciers using four ranges around the Snake River Plain. In the Tetons, they observed some correspondence between topography and glacial equilibrium line altitudes (ELA), but noted that local prominent peaks stand far higher than mean ELA. Foster *et al.* (2010) later proposed that 'teflon peaks' result from high rock competence and relatively fast uplift. Once formed, these peaks are preserved because steep slopes limit snow accumulation and cirque formation. They are also partly sustained by generating an orographic barrier, which focuses precipitation on the flanks and enhances deep, widely spaced glacial valleys. This implies that a literal interpretation of the 'glacial buzzsaw' fails in the Tetons. Foster *et al.* (2010) further explained how feedbacks between glaciers and topography (e.g. precipitation, insolation) control gross

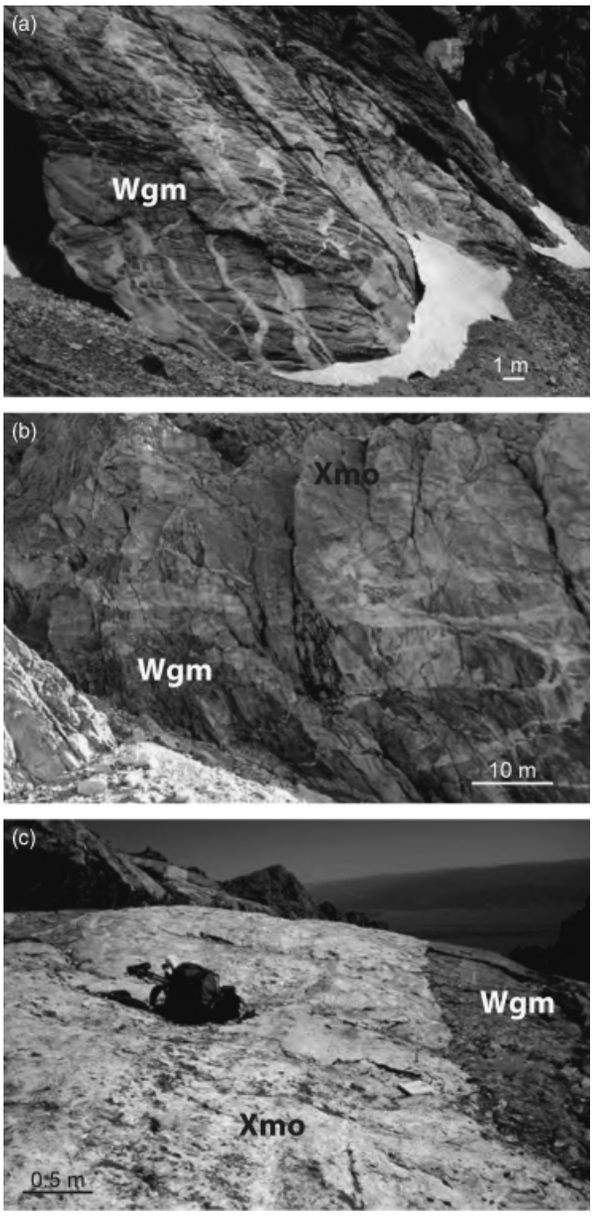

Fig. 3. Typical bedrock lithologies in Garnet Canyon. The two primary units are complexly intermixed. (a) Layered gneiss (Wgm) below North Fork with pegmatite inclusions. (b) Intermixed monzonite and gneiss in North Fork. (c) Sharp contact between monzonite and gneiss in South Fork.

valley morphology. In their conceptual model, glacial valleys reach a size threshold at which incision and headwall retreat push the divide west of the range crest. They also suggested summits are currently limited by hillslope erosion (i.e. at a threshold for mass wasting or in topographic steady state) (Burbank *et al.*, 1996; Willett & Brandon, 2002), such that the spacing of large glacial valleys dictates the heights of 'teflon peaks.' Although Foster *et al.* (2010) suggest a topographic steady-state for the range, most Teton peaks have experienced less denudation than valleys since uplift initiated.

Our study evaluates spatial and temporal efficiencies of erosional processes and onset of steady-state topography in Garnet Canyon, an $\sim$8 km^2 mixed glacial-fluvial catchment (Fig. 1). This canyon is classified as a mid-sized (type II) valley by Foster *et al.* (2010), in which significant relief has been generated by valley glacier incision, but without major headwall retreat. Canyon walls are steep and commonly extend up to 500 m, with slopes $> 60^\circ$ (Figs 2 and 4). The total relief of the catchment is 2 km, and its divide runs through the highest peak of the range. Active rock falls are common, and the valley bottom is partially buried by extensive talus. The basin was fully glaciated during the LGM with an ELA of $\sim$2600 m (Foster *et al.*, 2008), whereas today only small snowpacks and glaciers survive. An extensive terminal moraine at the foot of the basin suggests that past glacial erosion was highly efficient. Morphology alone, however, defines neither the spatial distribution of erosion across different altitudinal domains nor variations over time and climatic transitions. We propose two possible scenarios of erosion distribution in Garnet Canyon. First we hypothesize that erosion remained primarily focused at low elevations during both glacial and post-glacial times, increasing topographic relief. Alternatively, post-glacial erosion was focused at high altitudes due to destabilization of bedrock slopes, reducing relief as suggested by talus deposits. Observations of over-steepened valley walls and flattened valley bottoms make spatially uniform erosion over the short-term unlikely (Kirkbride & Matthews, 1997; Whipple *et al.*, 1999), and we expect that any snapshot of erosion given by detrital thermochronology will show focused erosion at some altitudinal zone.

METHODS

Sample collection

To quantify the variation in erosional efficiency under glacial and inter-glacial conditions, we sampled detrital sediment from an active stream and an $\sim$14 ka moraine deposit at the mouth of Garnet Canyon. Fluvial sediment was collected just above the outlet of the modern trunk stream into Bradley Lake (Fig. 5a). Approximately 3 kg of loose sand was scooped from a small sandbar, but was not panned in the field. Glacial sediment was collected from the steep inner moraine slope, about halfway up the innermost ridge of the Bradley Lake moraine (Fig. 5a). This $\sim$3 kg sample was collected by shovel after removing the outer $\sim$25 cm of sediment and soil, and sieved in the field to remove particles larger than coarse sand. An analysis of cobble lithologies in the moraine at this site indicated that all sediment was sourced from within Garnet Canyon and was not mixed with deposits in the Jackson Hole basin (supporting information). Both samples were refined using a Wilfley table and sieved to 63–250 μm, yielding $\sim$2.8 kg of sand in each sample. Samples were further purified using heavy liquids and magnetic separation, and dated as described below.

Five bedrock samples were collected, with four sample locations in the main trunk of the canyon (Fig. 5a) and

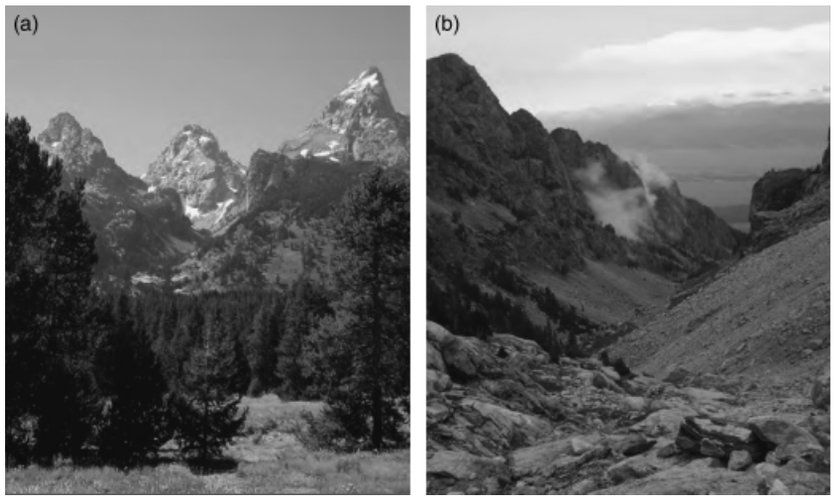

Fig. 4. Photographs of Garnet Canyon. (a) View looking west into Garnet Canyon from Jackson Hole. The peaks from left to right are Nez Perce, Middle Teton, and Grand Teton. This perspective shows the U-shaped valley in the canyon. A small cirque sits below Nez Perce. (b) View looking east into Garnet Canyon from the South Fork. The center of the image shows a small grassy area of alluvium. Beyond that, extensive talus fans from the north and south hillslopes cover the floor and stream channel. Bedrock in the foreground is glacially polished.

one location just below the sedimentary unconformity in Teton Canyon ~9 km from Garnet Canyon (Fig. 1). This sample was used to approximate maximum cooling age from the highest point of Garnet Canyon, given that we were unable to obtain a sample from the Grand Teton. It is likely that only minor erosion of crystalline rock (~100 m) has occurred above the Grand Teton, based on the unconformity projection above the range (Love *et al.*, 2003; Brown, 2010). This sample should constrain the upper part of the age-elevation relationship, although some uncertainty is associated with strata thickness and potential faulting between Garnet Canyon and the TT-1 sample location.

(U-Th)/He thermochronometry

The apatite (U-Th)/He thermochronology (AHe) technique is based on radiogenic production and thermally controlled diffusion of ^{4}He within host minerals. Apparent AHe cooling ages typically correspond to closure temperatures of ~70 °C, but closure temperature is cooling-rate and grain-size dependent (Wolf *et al.*, 1996; Farley, 2000). Cooling ages can be influenced by radiation damage or high U concentrations in neighboring grains (Ehlers & Farley, 2003). AHe ages were measured at Virginia Tech using ≥ 70 μm diameter grains that were handpicked from mineral separates at × 100 magnification. Pristine, inclusion-free apatites were generally used, although poor quality and yield was an issue for some samples. Aliquots were outgassed twice in Pt tubes in a resistance furnace at 940 °C for 20 min and analyzed for ^{4}He by ^{3}He spike and quadrupole mass spectrometry. Blank levels for ^{4}He detection are ~0.2 femtomoles, but none of the samples we observed had low ^{4}He levels. Radiogenic parent isotopes (^{238}U, ^{235}U, and ^{232}Th) were measured at Caltech and the University of Arizona by isotope dilution (^{235}U and ^{230}Th spike) and inductively coupled mass spectrometry (ICP-MS). Although ^{4}He is also produced by ^{147}Sm, it was not measured because it produces < 1% of radiogenic ^{4}He in typical apatite and should only be significant when U concentrations are < 5 ppm (Farley & Stockli, 2002).

Analytical uncertainty in ages is ~5% (1σ), based on instrument precision and error in the alpha ejection correction (Farley *et al.*, 1996). Accuracy was checked against routine measurement of known standards including Durango fluorapatite (30.9 ± 1.53 Ma, 1σ; $n = 40$), with a known AHe age of 31.4 Ma (McDowell *et al.*, 2005). Bedrock analyses were repeated 5–10 times per sample to characterize variability of single grain AHe ages from one sample. All ages from glacial and fluvial sediment are based on single grain age determinations. Previous studies indicate that ≥ 50 ages are needed to characterize a PDF from a detrital sample (Brewer *et al.*, 2003; Vermeesch, 2004; Ruhl & Hodges, 2005). We measured 103 detrital AHe ages from fluvial sediment and 67 ages from glacial moraine sediment. Using current methods, each individual detrital age measurement required ~2 h of cumulative effort, including grain preparation.

Bedrock ages (Table 1) were used to determine the age-elevation relationship in Garnet Canyon through linear regression. This relationship was calculated both with and without TT-1 to consider uncertainty related to the distance between sample collection sites. The relationships were applied to elevation data in a 10 m USGS digital elevation model (DEM) to estimate the age of bedrock surfaces throughout the catchment. We approximated horizontal isochrons, although they may dip gently westward as indicated by the orientation of the unconformity (a dip of ~10° produces a difference of only ~1 Ma). To find the PDF, the probability (P) of ages (t) were calculated using the equation of Stock *et al.* (2006) and Ruhl & Hodges (2005):

$$P(t) = \frac{\sum_{i=1}^{n} \left(\frac{1}{\sigma_{t_i}\sqrt{2\pi}} \right) e^{\frac{-(t-t_i)^2}{2\sigma_{t_i}^2}}}{n}.$$

The individual grain age is t_i, and the number of grains is n. For uncertainty (σ) we used both 10 and 20% (uncer-

Table 1. AHe data for bedrock

Sample	Elevation (m)	Latitude (N)	Longitude (W)	Rock type	Mass (mg)	MWAR (μm)	He (pmol)	U (ppm)	Th (ppm)	No. of grains	F_T	Corr. Age (Ma)	Average Age (Ma)	Standard Deviation	% Error
TT-1	2132	43.7561	110.9155	Granitoid	0.0063	49.9	0.0446	25.2	3.6	2	0.75	69.6			
					0.0169	*60.4*	*0.4177*	*41.4*	*18.1*	*4*	*0.78*	*131*			
					0.0188	68.3	0.0768	14.0	4.0	4	0.81	64.3	60.9	9.82	16.1
					0.0222	82.9	0.2007	29.8	10.7	2	0.85	62.7			
					0.0208	68.0	0.1230	27.7	5.8	3	0.83	46.8			
TT-2	3385	43.7346	110.8074	Layered gneiss	0.0036	32.7	0.4250	50.3	32.9	4	0.62	61.8			
					0.0092	40.0	0.1649	62.7	39.5	6	0.69	68.2			
					0.0297	57.8	0.4157	42.1	26.4	8	0.79	70.0	61.8	22.7	36.8
					0.0497	*81.3*	*0.3534*	*13.5*	*4.0*	*5*	*0.86*	*108*			
					0.0067	37.6	0.0614	48.1	30.2	5	0.67	47.1			
TT-2	3385	43.7346	110.8074	Layered gneiss	0.0019	41.4	0.0360	70.6	48.6	1	0.72	61.0			
					0.0006	27.6	0.0047	44.8	28.3	1	0.59	52.9			
					0.0015	46.0	0.0103	29.4	19.5	1	0.73	50.6	54.0	15.9	29.4
					0.0005	27.6	0.0056	76.1	49.1	1	0.53	44.7			
					0.0008	*32.2*	*0.0090*	*31.1*	*17.5*	*1*	*0.60*	*96.5*			
					0.0009	*32.2*	*0.0167*	*59.6*	*35.3*	*1*	*0.64*	*78.8*			
					0.0007	27.6	0.0055	37.3	22.5	1	0.59	61.3			
					0.0008	23.0	0.0149	95.3	46.8	1	0.54	59.9			
					0.0022	41.4	0.0206	40.4	23.0	1	0.72	55.1			
					0.0017	41.4	0.0096	29.3	17.8	1	0.71	46.5			
TT-4	2985	43.7288	110.7926	Quartz monzonite	0.0036	28.6	0.0243	99.8	52.6	7	0.59	19.4			
					0.0074	46.6	0.0265	36.4	30.7	5	0.74	21.2			
					0.0141	58.8	0.0919	66.2	4.2	4	0.78	23.6	21.4	2.11	9.8
					0.0082	*44.3*	*0.0710*	*43.7*	*9.9*	*5*	*0.73*	*49.6*			
					0.0028	*33.0*	*0.0267*	*84.3*	*10.4*	*3*	*0.63*	*33.7*			
TT-5	2853	43.7260	110.7910	Layered gneiss	0.0024	69.0	0.0050	15.5	2.8	1	0.74	34.3			
					0.0055	*133.4*	*0.0083*	*9.8*	*0.3*	*1*	*0.78*	*37.9*			
					0.0039	115.0	0.0129	24.6	1.9	1	0.75	33.5	25.8	5.42	21.0
					0.0071	105.8	0.0125	15.1	1.1	1	0.82	27.1			
					0.0047	115.0	0.0139	25.7	2.9	1	0.77	27.5			
					0.0085	*147.2*	*0.0167*	*7.7*	*0.0*	*1*	*0.81*	*60.8*			
					0.0024	69.0	0.0025	12.9	0.0	1	0.74	21.5			
					0.0024	69.0	0.0042	20.3	0.0	1	0.74	22.5			
					0.0017	*59.8*	*0.0035*	*8.5*	*0.1*	*1*	*0.71*	*67.3*			
					0.0045	*69.0*	*0.0122*	*15.6*	*1.7*	*1*	*0.79*	*41.0*			
					0.0011	36.8	0.0008	12.3	1.2	1	0.68	16.6			

Table 1. (Continued)

Sample	Elevation (m)	Latitude (N)	Longitude (W)	Rock type	Mass (mg)	MWAR (μm)	He (pmol)	U (ppm)	Th (ppm)	No. of grains	F_T	Corr. Age (Ma)	Average Age (Ma)	Standard Deviation	% Error
					0.0014	32.2	0.0013	11.0	1.0	1	0.63	25.6			
					0.0010	32.2	0.0032	31.2	4.6	1	0.65	29.6			
					0.0009	32.2	0.0010	15.0	0.0	1	0.64	20.6			
					0.0017	32.2	0.0031	22.3	0.9	1	0.64	24.5			
TT-8	2461	43.7237	110.7639	Quartz monzonite	0.0042	42.8	0.0036	28.2	11.3	4	0.70	7.62			
					0.0063	*49.8*	*0.0489*	*48.1*	*7.1*	*6*	*0.77*	*15.0*			
					0.0168	69.8	0.0056	16.0	4.5	3	0.82	4.55	11.3	5.22	46.1
					0.0249	*89.6*	*0.0415*	*10.8*	*249*	*2*	*0.87*	*21.7*			

Ages in italics were outliers excluded from average age calculation. Standard deviation is 1σ. MWAR is mass-weighted average of aliquots and radius of single grains. FT is alpha ejection correction factor.

tainties for typical AHe results and samples in this study respectively). The DEM estimated age distribution PDF is a predictive model of uniform erosion conditions that will be compared with the observed glacial and fluvial data (Brewer *et al.*, 2003; Ruhl & Hodges, 2005; Stock *et al.*, 2006). Deviations from the model will indicate how these erosion mechanisms recently influenced relief within Garnet Canyon.

To test for the statistical strength of differences between these PDFs, we implemented a Kuiper equality test (Kuiper, 1960; Stephens, 1965; Ruhl & Hodges, 2005; Stock *et al.*, 2006). This technique calculates the sum of the distance between two PDFs (Kuiper statistic, K) and corrects for sample size to get an asymptotic K (Ka). The fluvial and glacial PDFs were compared with each other and to the predicted curve. Ka was also computed for randomly generated distributions of ages from the predicted age distribution to assess the observed differences between samples and the map prediction. This test can be further augmented using a Monte Carlo model (see supporting information for detailed methods).

Apatite quality studies

While the detrital age distributions potentially record vertical variation in erosion, the effect of apatite quality on PDFs can be problematic in small basins because AHe ages are susceptible to inaccuracy due to the presence of micro- and submicroscopic inclusions (zircon, monazite, etc.), parent isotope zonation, grain size variation, microfractures, radiation damage, contamination by neighboring minerals, and local surface thermal events (e.g. forest fires) (Farley *et al.*, 1996; House *et al.*, 1997; Reiners & Farley, 2001; Ehlers & Farley, 2003; Jolivet *et al.*, 2003; Mitchell & Reiners, 2003; Boyce & Hodges, 2005; Fitzgerald *et al.*, 2006; Green *et al.*, 2006; Stock *et al.*, 2006; Reiners *et al.*, 2007; Emmel *et al.*, 2008; Flowers, 2009; Flowers *et al.*, 2009). Several tests evaluated the effects of variable apatite yield and quality on detrital age distributions. First we studied the innate reproducibility of single grain ages by measuring a high number (10, 15) of replicates of two bedrock samples (TT-2, TT-5). Because each grain within a bedrock sample should have the same cooling history, this quantifies the variation in a detrital PDF due to inherent uncertainty in AHe ages, as opposed to the spatial distribution of erosion. We also characterized apatite yield in the two primary lithologies of Garnet Canyon. Three samples of monzonite and two samples of gneiss were processed using identical mineral separation techniques to measure the concentration of datable apatite grains. Apatite yields were measured as the mass of nonmagnetic grains (density $> 3.0\,\mathrm{g\,cm^{-3}}$), multiplied by the fraction of a separate consisting of apatite (based on point counts, $n = 100$), and normalized by the original mass of the rock sample. The percentage of apatite grains of datable quality was also determined using the standard selection criteria of grain size, crystal form, optical quality, and lack of inclusions.

Apatite quality from representative samples was also determined by examining grains for inclusions smaller

than 5 μm and zones of heavy elements (U, Th, etc.) using scanning electron microscopy (SEM) and cathodoluminescence (CL). Apatite grains with zircon or monazite inclusions have higher U and Th concentrations that are not fully measured by standard dissolution techniques, and produce excess helium that results in anomalously old ages. Zonation results in overestimating or underestimating the cooling age if U or Th is concentrated in the core or rim, respectively (Reiners & Farley, 2001; Jolivet *et al.*, 2003; Spotila *et al.*, 2004; Emmel *et al.*, 2007, 2008; Haeussler *et al.*, 2008).

Apatite grains from one gneiss sample, one quartz monzonite sample, and the fluvial sediment sample were mounted in epoxy and scanned for inclusions and zonation using a CamScan Series 2 SEM. We scanned ~50 grains in each sample for the presence of inclusions, inclusions with zircon, and zones. We specifically searched for inclusions smaller than ~5 μm, which would be too small to be screened using optical microscopy. Inclusion composition was determined by energy-dispersive spectrometry (EDS). Compositional zonation was imaged using backscatter electron (BSE) imaging and CL. These techniques are sensitive to heavy atomic mass isotopes, although specific concentrations were not measured.

Corrections to the predicted age distributions were made using the methods of Amidon *et al.* (2005) to correct for apatite yield and quality. Separate PDFs were calculated for the gneiss and monzonite. The fractional areas of the gneiss and quartz monzonite were determined with a geologic map in ArcMap (Fig. 5) (e.g. gneiss area divided by total area). The fractional apatite yields were measured as discussed above (Table 2). A separate area-concentration factor was calculated for each bedrock unit by multiplying the fractional apatite yield by the fractional bedrock area, which was next multiplied to the PDF. Finally, the PDFs from each rock unit were added to create the corrected PDF.

RESULTS

Basin hypsometry

The hypsometry of Garnet Canyon, determined with 10 m resolution digital elevation models in ArcMap, is shown in Fig. 6. Elevations range from ~2200 to 4198 m. The frequency of elevation increases steeply around 2900 m and decreases rapidly above 3500 m, with a relatively even distribution of elevations in between. The box-like shape of the canyon-wide hypsometry reflects typical moderate glaciation compared with alpine catchments in other

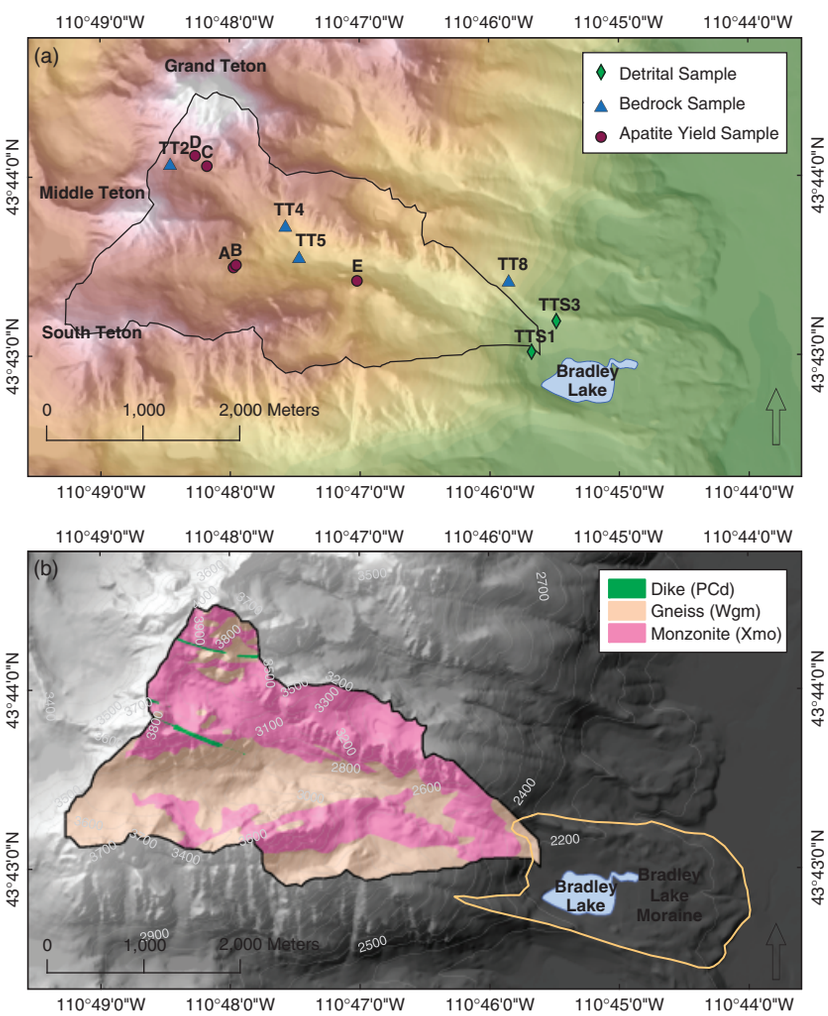

Fig. 5. Maps of Garnet Canyon including sample locations and geology. (a) Map of sample locations on a 10 m resolution digital elevation model with shaded relief of Garnet Canyon. (b) Geologic map of Garnet Canyon was based on data from Love *et al.* (1992), showing the distribution of monzonite and gneiss exposed throughout the basin and projected below talus, glaciers, and snow packs. The yellow line indicates the extent of the LGM moraine. Note that variation occurs within mapped units, as shown in Fig. 3, such that bedrock sample lithology may vary from what has been mapped at that location (e.g. samples A and B).

Table 2. Apatite yield and quality summary

Sample	Rock type	Apatite Yield (mg kg^{-1})	Yield with euhedral form (mg kg^{-1})		Yield with 2 pyramidal terminations (mg kg^{-1})		Yield without inclusions (mg kg^{-1})	
(a) Apatite yield								
WT-A	quartz monzonite	0.33	0.30	91%	0.00	0%	0.12	36%
WT-B	quartz monzonite	0.17	0.16	95%	0.00	0%	0.07	40%
WT-C	quartz monzonite	0.17	0.17	100%	0.00	0%	0.00	0%
WT-D	gneiss	370	320	86%	35.0	9%	170	47%
WT-E	gneiss	160	150	94%	17.9	11%	41	26%
TT-1	quartz monzonite	34						
TT-2	gneiss	600						
TT-4	quartz monzonite	2.1						
TT-5	gneiss	1400						
TT-8	quartz monzonite	80						

Sample	Description	No. of grains analyzed	% with zonation	% with inclusions	% with inclusions <5 μm	% with zircon inclusions	% outliers from age calculations
(b) Apatite zonation and inclusions based on SEM and CL							
TT-2	Gneiss	50	73	66	34	6	20
TT-8	Quartz monzonite	50	10	76	34	8	50
TTS-1	Fluvial sediment	41	39	12	7	5	24

regions (Brocklehurst & Whipple, 2004). The majority of elevation is above the last glacial maximum ELA (~2600 m, Foster *et al.*, 2008).

The elevation distribution represented by each major bedrock unit in the catchment is also shown (Fig. 6). Given that colluvial deposits cover one-third of the surface area of the basin, we projected bedrock beneath areas of talus cover (Fig. 5b). The resulting bedrock area shows that layered gneiss and quartz monzonite have approximately equal distribution across altitudes in the basin. The distribution of each bedrock type is also roughly uniform with elevation, such that the hypsometries for gneiss and monzonite are basically similar and mimic that of the entire basin. The gneiss in particular has a very uniform elevation frequency between 2750 and 3500 m. Since variability in elevation represented by bedrock units may affect the distribution of detrital cooling ages, we corrected PDFs for the hypsometry of each rock unit. The comparable hypsometry of the two bedrock units should reduce the bias of differentiated apatite yield.

Apatite (U-Th)/He thermochronometry

Bedrock AHe cooling ages increase with elevation (Fig. 7). The relationship is roughly linear with a possible change in slope approaching older ages as expected from results of apatite fission-track studies (Roberts & Burbank, 1993; Brown, 2010). While the small age difference between the uppermost samples may represent a change in cooling history, it could also result from different cooling histories associated with the horizontal distance between sampling locations. The linear relationship produced without sample TT-1 is also illustrated in Fig. 7. The maximum AHe age for the basin was assumed to be equal to the cooling age of basement just below the Paleozoic unconformity (TT-1, 60.9 Ma) (Table 1). The oldest apatite fission track (AFT) age recorded by Roberts & Burbank (1993) in the range is 82.5 Ma on Rendevous Peak. Since AFT ages are typically older than AHe ages, our results in Garnet Canyon appear reasonable. Overall reproducibility of bedrock ages is poorer than observed in other recent AHe studies. Errors reported for bedrock average AHe ages are standard deviations of replicate analyses (Table 1), which averaged ~22% (1σ, $n \geq 2$), whereas ~10% is more typical (Berger *et al.*, 2008; McAleer *et al.*, 2009). In addition, each bedrock sample yielded anomalous ages that were culled before averaging (e.g. 1 age in sample TT-1 was twice as old as the other four ages; Table 1). Anomalously old ages are assumed to result from either contamination by inclusions or zonation, the former of which is indicated in the majority of anomalous ages by helium outgassing during re-extraction. Of 44 bedrock age determinations, 12 ages were considered outliers and culled from the data before averaging (27%). No significant difference in reproducibility was observed between multigrain and single grain bedrock age (Table 1).

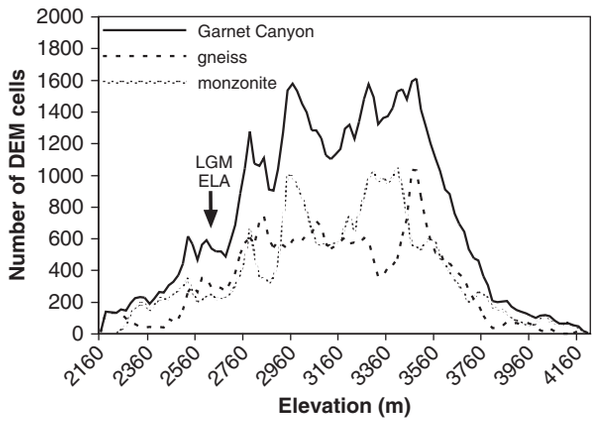

Fig. 6. Elevation hypsometry for Garnet Canyon. Solid black line is the elevation hypsometry of the entire area in the basin. Black dashed line is the hypsometry of areas mapped as gneiss. Gray dotted line is the hypsometry of areas mapped as monzonite. Hypsometries were calculated from a 10 m DEM and geology areas were extracted from the distribution of units shown in Fig. 5b. The arrow points to the approximate location of the equilibrium line altitude (ELA) during the last glacial maximum (LGM) estimated by Foster *et al.* (2008).

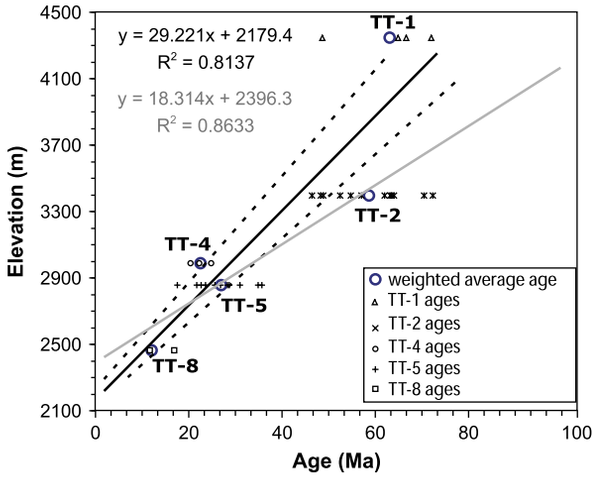

Fig. 7. Age–elevation relationships for bedrock AHe samples in Garnet Canyon. The solid black line is the linear regression including all samples and the dashed lines indicate 1σ uncertainty. Individual aliquot or single grain ages are included for each sample (Table 1). The relationship shown in black was used to generate the predicted PDF based on basin hypsometry. Since sample TT-1 was taken from outside of Garnet Canyon at the top of the basement (Fig. 1a), the solid gray line shows the linear regression created excluding TT-1. The equation in gray text corresponds to this line.

Histograms of detrital AHe ages from the sediment samples show an age range that mostly falls between maximum and minimum bedrock ages (Fig. 8 and Table 1). Given that the maximum bedrock age is ~61 Ma, and uncertainties on bedrock ages averaged ~22% (1σ), we considered any detrital age >80 Ma to be spuriously old. One age was culled because it was anomalously young relative to the lowest bedrock sample. Of 170 single grain age determinations, 33 were culled (18%; Table 2), which is consistent with the occurrence of outliers in the bedrock ages. Curiously, more ages were culled from the fluvial sediment sample (25%) than from the glacial moraine sample (10%). Although each detrital grain originated from a different location in the basin, the average age of either population provides a rough measure of the mean elevation from which grains were sourced.

Although we did not measure ^{147}Sm on these samples, all apatite grains showed U concentrations above ~10 ppm (average of all 214 age determinations is 36 ppm), such that ^{147}Sm should not be responsible for a significant fraction of radiogenic ^{4}He (Farley & Stockli, 2002). Note that one gneiss sample (TT-5) and numerous detrital grains exhibited low or even negligible Th concentrations. Measured AHe ages show no correlation to effective U (eU) or grain size (MWAR or radius; Fig. 9). This suggests radiation damage and variations in diffusivity related to grain radius are not significant factors in the overall age distribution (Reiners & Farley, 2001; Meesters & Dunai, 2002; Flowers, 2009; Shuster & Farley, 2009).

Apatite yield and quality

Monzonite samples yielded an average of 0.22 mg of apatite per kilogram of rock, whereas gneiss samples yielded an average of 270 mg of apatite per kilogram of rock (Table 2). When combined with other dated samples for which we have rough estimates of yield, the average yields are 19 mg and 620 mg kg^{-1} of rock for monzonite and gneiss, respectively (six monzonite and four gneiss). The samples specifically collected for measuring apatite quality were carefully assessed with a point count of 100 grains, while the apatite yield from the dated samples were roughly estimated from grains in a sample dish and may be an overestimation. The difference between these estimates indicates that heterogeneity exists within both lithologies, but both estimates show that gneiss has at least 33 times more apatite per kilogram of rock. Apatite quality was poor in monzonite samples based on observations that none of the grains showed good crystal form and many grains exhibited a high occurrence of opacity and discoloration. In contrast, ~10% of the apatite grains in gneiss were approximately euhedral with two pyramidal terminations (Table 2b). Scanning grains for inclusions revealed an average of 78% of the quartz monzonite grains and 64% of the layered gneiss grains contained visible inclusions greater than 5 μm (Fig. 10). If these results are representative of all bedrock from Garnet Canon, they effectively mean that nearly all dated detrital apatite grains were sourced from the half of the catchment area consisting of gneiss bedrock. While detailed observations of dated grains were not recorded, both fluvial and glacial samples contained enough euhedral to anhedral grains to easily pick a sufficient quantity for detrital dating.

Further examination of three dated samples (TT-2, TT-8, and TTS-1) investigated the apatite quality and potential causes of anomalously old ages. A significant fraction

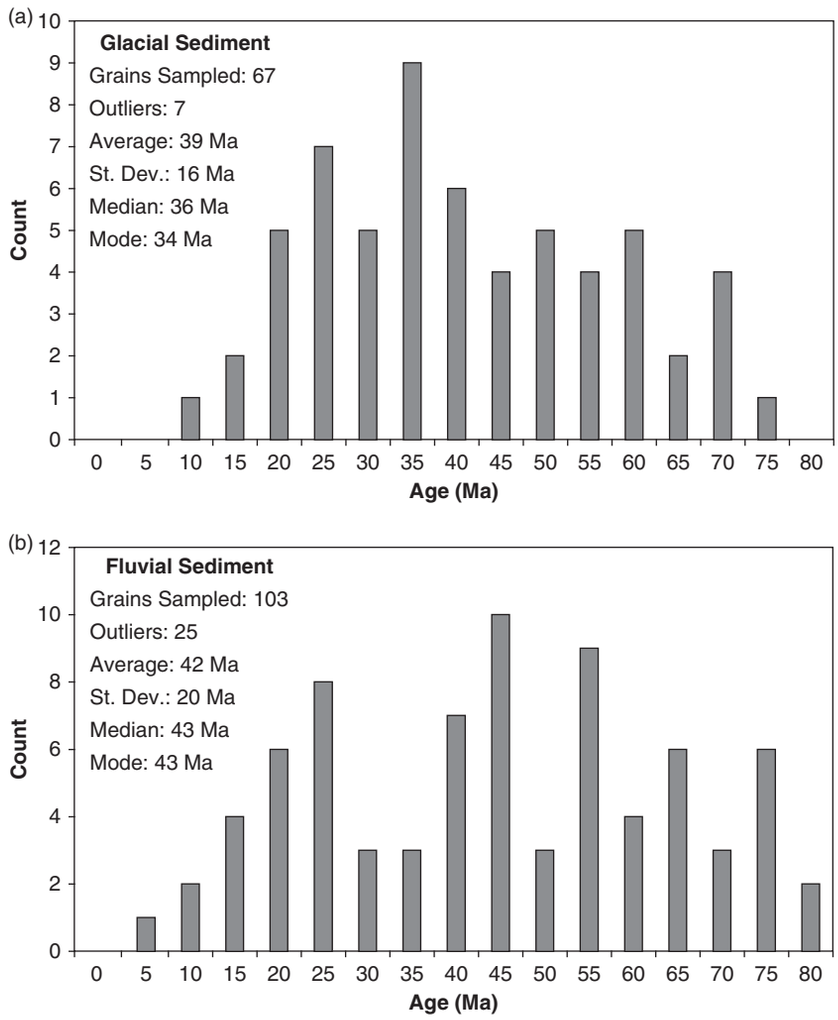

Fig. 8. Histogram of detrital AHe ages from glacial and fluvial sediment samples. Ages older than 80 Ma are considered outliers and are excluded from the graphical representation and statistical summary.

of apatite crystals in each sample exhibited compositional zonation on CL or SEM (Table 2b). Images show zoning was most common in apatite from the layered gneiss (Table 2b and Fig. 10), where cores were bright relative to rims (Fig. 10). This pattern of concentrated U or Th would lead to an over-estimate of alpha ejection and an overestimate of corrected AHe ages (Farley *et al.*, 1996; Spotila *et al.*, 2004; Haeussler *et al.*, 2008). In the monzonite and fluvial sediment samples, roughly half of the grains had higher atomic masses near the center of the grain, while the remaining half showed these concentrations along the rim in CL.

Inclusions were also frequently observed in each sample (Table 2b). On average, ~35% of the inclusions were submicroscopic (< 5 μm), and thus would not be visible to screening with the optical microscope. Overall, inclusions were less frequent in the detrital sand than in bedrock samples, suggesting that grain durability limits the presence of inclusions in detrital sand (Kowalewski & Rimstidt, 2003), consistent with observations that inclusions tend to be associated with fractures or flaws in crystals. Fewer than 10% of the grains contained submicroscopic zircon inclusions and could be responsible for a fraction of the anomalously old AHe ages observed and treated as outliers. Other inclusion compositions included silica, iron, or other elements common in apatite, suggesting that the majority of inclusions observed during optical screening probably do not affect AHe ages (Buscher & Spotila, 2007). In any given sample, undetected zircon inclusions, together with concentrations of parent isotopes in the grain core could result in an over-estimate of the AHe cooling age. It is interesting to note, however, that despite differences in the quality observations among the three samples, the occurrence of AHe age outliers was comparable from sample to sample (Table 2b).

Probability density functions (PDFs)

PDFs were calculated for age-elevation predicted and detrital age populations. Based on single grain bedrock age reproducibility in this and previous studies, we used uncertainties of 20 and 10% (1σ). The predicted distribution of ages based on the bedrock derived age-elevation gradient and basin hypsometry was calculated both alone and corrected for the difference in apatite yield between gneiss and monzonite (Fig. 11a). Although the difference in apatite yield is large, these curves are similar due to the equal distributions of gneiss and monzonite across eleva-

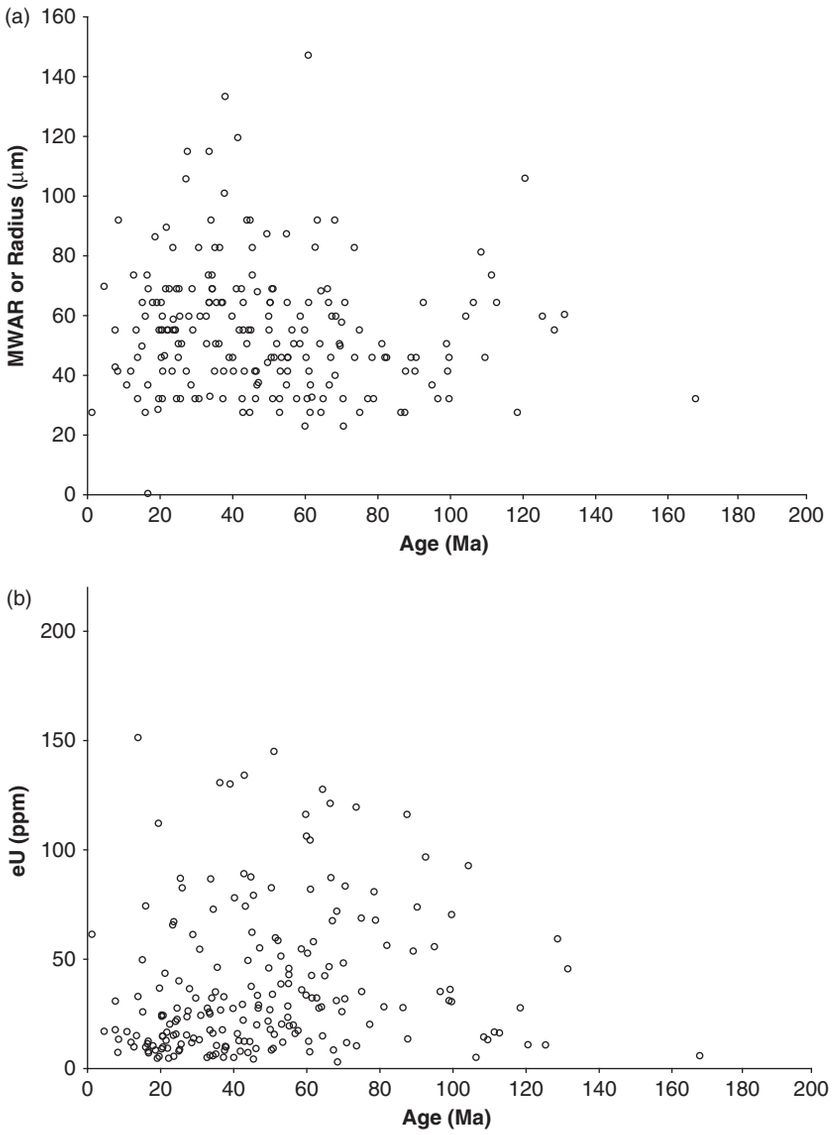

Fig. 9. Plots of AHe age versus grain radius and eU. No correlations exist between age and (a) grain radius of individual grains or mean weighted average radius (MWAR) in bedrock aliquots or (b) eU concentrations. Graphs include all bedrock and detrital ages measured, excluding values greater than 200 Ma ($n = 205$).

tions (Figs 5b and 6). The observed PDFs of glacial and fluvial detrital ages are shown in comparison to the predicted distribution corrected for yield (Fig. 11b and c). The glacial PDF is roughly bell-shaped and peaks around 35 Ma. The fluvial PDF is bimodal, with peaks at ~22 and 42 Ma and a gap in ages at ~30 Ma.

The bulk of ages range between 15 and 50 Ma in all PDF curves, yet differences between them are significant. The glacial and fluvial PDFs exhibit higher occurrence of ages $\geq$ 50 Ma than the predicted PDF. This may represent a concentration in erosion at high altitude, a systematic over-estimate in AHe age due to quality, or an underestimation of the proportion of older ages based on linear gradient assumptions for the predicted PDF. When the predicted PDF curve was calculated with the linear gradient excluding sample TT-1 (Fig. 7) and compared with the sediment curves, it also showed a higher than expected occurrence of old ages in the fluvial sediment (Fig. S3 in supporting information). The peak around ~8 Ma may be associated with assigning uncertainty as a percentage of the age. The glacial and fluvial PDFs vary with each other in the observed occurrence of ages ~25–40 Ma. Note that PDFs generated using 20% (1σ) error bars produce smoother curves from the same data, although the same basic differences remain (Fig. 11c).

Results show that fluvial and glacial detrital age PDFs are statistically different from one another. The glacial and fluvial distributions both differ from the predicted distribution. The Monte Carlo simulation indicates that observed differences in age distributions of fluvial and glacial grains are highly significant for both 10 and 20% uncertainty levels, consistent with the Kuiper test (see supporting information for detailed table and distributions of Kuiper asymptotic statistic).

DISCUSSION

Spatial variation of erosion in Garnet Canyon

The PDFs created from detrital AHe ages identify similarities and distinctions between glacial and fluvial sediment

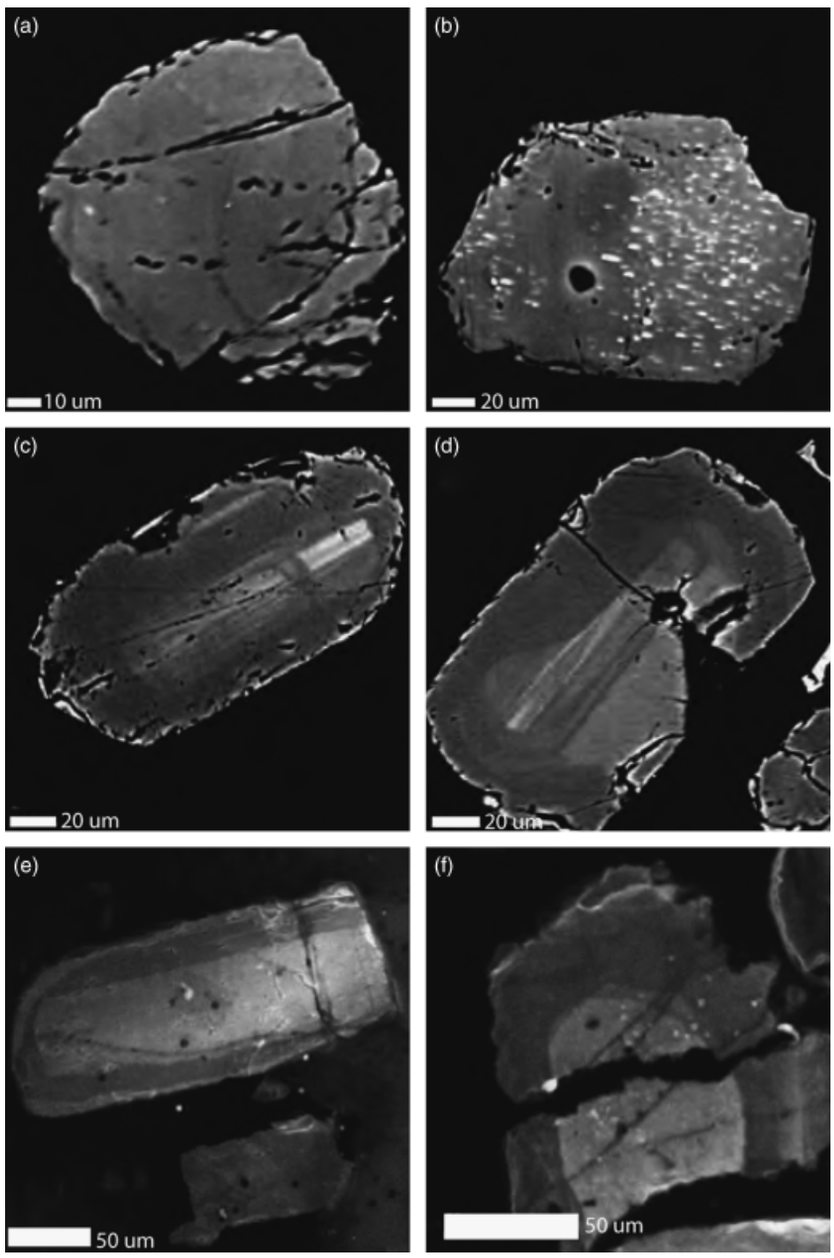

Fig. 10. Examples of apatite grains illustrating the prevalence of inclusions and zonation. SEM images (a) and (b) show small, bright inclusions in apatite grains from bedrock sample TT-8. These inclusions are too small to be observed with an optical microscope. SEM images (c) and (d) show zonation from apatite grains in bedrock sample TT-2, with bright zones occurring near the core. CL images (e) and (f) also show zonation in apatite grains from sample TTS-1.

samples and the predicted age distributions. Fluvial and glacial PDF curves both attain their maximum probabilities within the broad peak of the predicted distribution; yet are statistically distinct. The statistical difference between the detrital age populations suggests that they effectively record information about erosional dynamics and variability through a glacial–interglacial climate shift in Garnet Canyon. The detrital age distribution in the glacial sample, as well as the mean and median, is slightly younger than those in the fluvial sample, suggesting the locus of erosion may occur at lower elevations in the glacial system (Fig. 11b). These differences are very subtle, however, and the ranges of the curves are similar in all three PDFs (Fig. 11b). The similarity between PDFs is even more pronounced when larger error bars are assumed (Fig. 11c). The increased similarities in shape may imply long-term uniformity across systems, however, statistical analyses and small distinctions between curves support short-term variability.

A large difference between observed and predicted PDF curves occurs in the upper part of the basin, or above ~55 Ma (Fig. 11b). The large area below the tail of both observed detrital curves represents a high frequency of grains sourced from elevations > 3700 m, unless these ages are a product of systematic age overestimation. If this signal correctly represents sediment derived from the upper part of the basin, it provides insight into erosional processes in this setting. First, it suggests that sediment routing in small basins can be effective, despite the potential overdeepenings formed by glacial erosion. Alluvial traps are not developed well enough to prevent sediment transport throughout this basin as observed in other ranges (Stock *et al.*, 2006; Duhnforth *et al.*, 2008). The small alluvial deposits in flattened reaches of Garnet Canyon

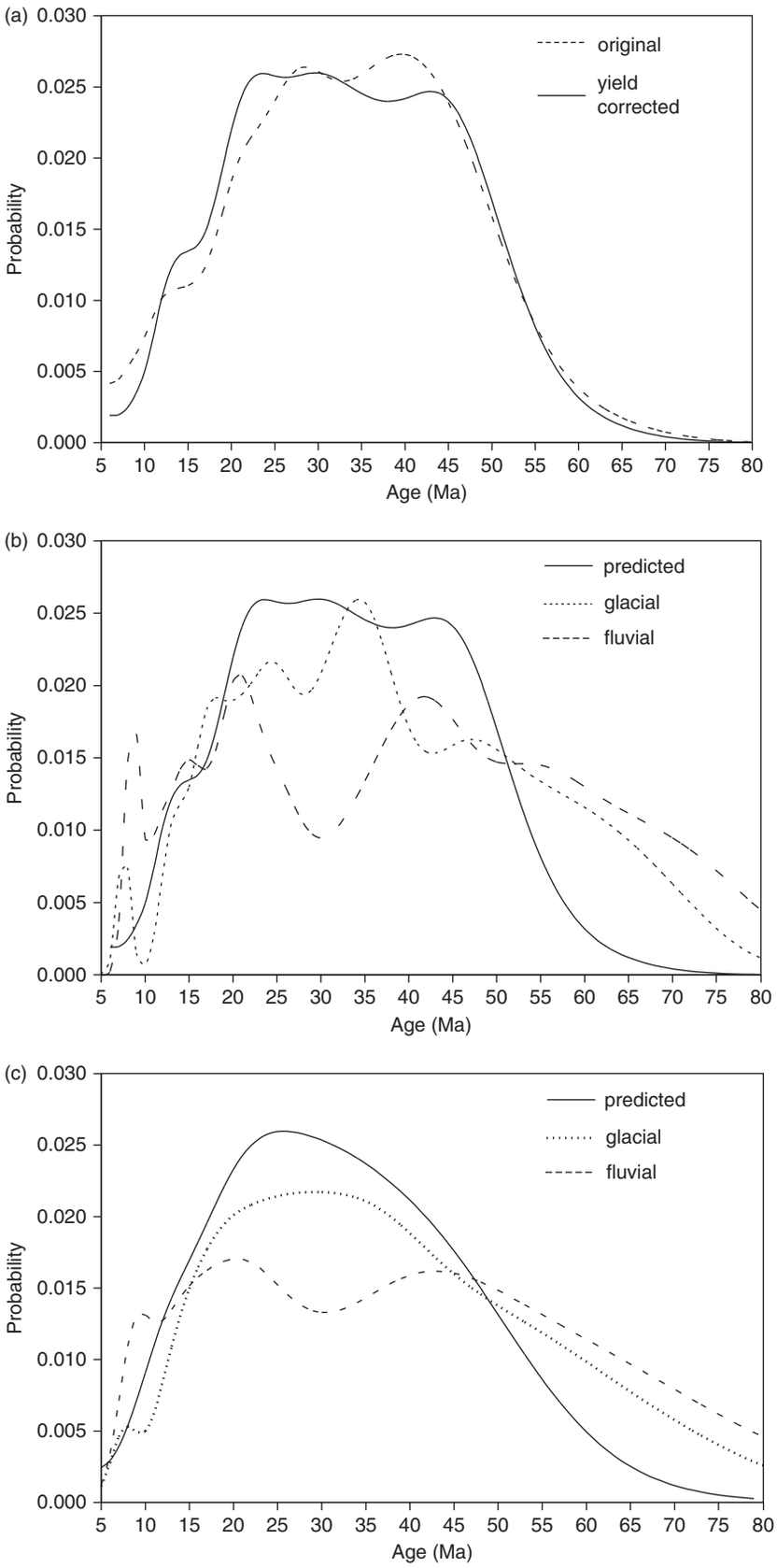

Fig. 11. PDF curves for Garnet Canyon. (a) The original PDF based on age-elevation gradient and elevation hypsometry (dashed line) is very similar to the corrected PDF based on bedrock surface area and apatite yield (solid) (Fig. 5b). (b) The glacial PDF (dotted line) and fluvial PDF (dashed line) are compared with the predicted PDF calculated with 10% uncertainty. Highest probabilities in all curves are within a similar age range. Both detrital PDF curves have tails that extend beyond the range of predicted ages. (c) PDF curves generated for the same values as (b) assuming 20% uncertainty.

apparently do not store sediment or prevent grains from higher elevations from reaching the mouth of the canyon. The coarse talus (2–10 m boulders) across the stream creates large void spaces allowing rapid flow and high discharge associated with seasonal snowmelt to evacuate unconsolidated sediment from higher reaches. Second, the older ages suggest that high elevations erode more aggressively than expected based on the age elevation predic-

tion. Surfaces at high altitudes represent only a small fraction of the catchment area, but contribute significant volumes of material to the sediment flux. One implication of this is that relief is being reduced or is at least limited due to mass wasting, both now and during glacial times (Straumann & Korup, 2009). This is true whether the detrital grains are weathering directly out of bedrock at high elevations, or if they are instead derived from ridge blocks now positioned on the valley floor.

The glacial PDF suggests that the mid-altitude region of the basin experienced erosion as the glacier advanced and contributed sediment to the end moraine (Fig. 11b). By sampling only the sand-sized particles, this signal may be biased toward abrasion occurring at the base of the glacier; however, it records that incision created unstable slopes, which resulted in rapid adjustment and deposition after glacial retreat. The fluvial sediment is mainly sourced from low elevations due to incision and high elevations due to the prevalence of talus, whereas the middle portion of the basin may not be a major source of sediment. This may be due to preferential erosion of talus cover previously mentioned, and a transport limited state at middle elevations (Fig. 4b). The distinction between the bell-shaped glacial PDF and bimodal fluvial PDF is important because it could represent variation in erosion patterns between two climatic regimes.

Implications for detrital dating techniques

Pioneering research and modeling in detrital thermochronometry and investigations of assumptions have allowed this technique to evolve into an effective tool to study landscape evolution (Stock & Montgomery, 1996; Brewer *et al.*, 2003; Ruhl & Hodges, 2005). Results from the Teton basins confirm that spatial variability in erosional processes can be preserved and recognized in the sediment record from a complex basin supporting the results of Stock *et al.* (2006) that detrital cooling ages can serve as markers of recent erosion. This also supports their suggestion that older deposits could provide a valuable geomorphic tool to evaluate erosion and relief history of basins. The glacial sediment record provides evidence of focused erosion at intermediate elevations and variation in erosion from the fluvial record.

The potential of detrital techniques for geomorphic and tectonic studies are limited by drawbacks, such as sampling bias and mineral quality, which could introduce error in PDF calculations. Previously, most studies assumed homogeneous distribution of datable mineral grains and the problem of variable quality was addressed by either selecting catchments of uniform lithology (Stock *et al.*, 2006) or correcting PDFs based on estimated mineral yields over large areas (Amidon *et al.*, 2005). Analyses of Teton samples reveal that approximately one in five measurements can be expected to be anomalously old and thus need to be culled from the data sets. A similar ratio of outliers appears in detrital ages (Table S1 in supporting information). Setting an age value that is 'too old' and excluding all measurements greater than this value partly resolves this issue. However, if the predicted age is too young due to the assumption of a linear relationship between samples TT-1 and TT-2, fewer outliers would be culled. With this study it was useful to evaluate the validity of the predicted ages by modeling ages with different linear relationships and comparing expected ages to results of previous studies. PDF curves calculated without TT-1 produced ages older than expected based on fission track studies (Roberts & Burbank, 1993) and still showed abundance of old ages in the fluvial sediment.

Results suggest that caution be used when using single 'grab-bag' detrital samples as proxies for bedrock age-elevation profiles to determine cooling and exhumation history. Detrital cooling age models assume that geomorphic conditions remain uniform throughout the interval of mineral cooling ages represented in a detrital sample (Brewer *et al.*, 2003; Ruhl & Hodges, 2005; Brewer & Burbank, 2006). Variability between detrital PDFs observed over a short interval highlights the sensitivity of this application to erosion variability, therefore assumptions of uniform erosion and steady-state topography may not accurately describe these systems (Ruhl & Hodges, 2005). If quality varies spatially in source bedrocks, detrital age distributions may over- or underestimate the probability of apatite being sourced from a particular elevation. The distribution of ages from modern sediment can yield information comparable to what could be learned from an altitudinal transect of bedrock cooling ages with careful thermokinematic modeling (Brewer *et al.*, 2006; Whipp *et al.*, 2009). In many cases, the exhumation history of a basin will be much easier to obtain via traditional bedrock sampling, which requires fewer analyses, produces replicate measurements to test for age reproducibility (Berger *et al.*, 2008), and will be less affected by transient landscape conditions.

This study also demonstrates the importance of mineral yield and quality in detrital thermochronology. Although apatite yield differs significantly between two lithologies in Garnet Canyon, the technique succeeded because the division between the two units is parallel to the length of the basin, thus producing similar elevation distributions for each. Further bias may be caused by a localized body of rock (e.g. large xenolith < 100 m) with relatively high apatite yield and exceptional apatite quality that could generate an artificial peak in the detrital PDF. Future studies should not assume homogenous distribution of datable grains, however, even in purely crystalline rock. Analyses of complex basins should include assessments of the hypsometry of individual rock units before sampling. Detailed analyses of grains with SEM and CL provide an estimate of the percentage of grains likely to produce outliers, which could be excluded from calculations without affecting results. Although the lithology is complex and apatite quality is poor in Garnet Canyon, this technique identified variations in erosional patterns and transitions associated with the recent change from glacial to fluvial conditions, thus showing that the detrital AHe technique is a useful geomorphological tool.

Unfortunately, SEM and CL analyses do not resolve the potential for systematic error to produce slightly older ages for a number individual grains, in which case areas with poor apatite quality simply may not be suitable for detrital AHe studies. The PDF calculation assumes no skewness in error bars; however, our observations of apatite quality suggest that more factors are likely to produce older ages than younger ages in samples from the Teton Range. A number of single grain ages could be older than the mean cooling age of their respective source bedrock, yet if they still fall within the acceptable age limit based on the oldest AHe age in the basin and its associated error, they will not be excluded from the data set. This is a potentially serious flaw. Further investigation would be required for us to determine whether the large fraction of older ages represents concentrated erosion at high elevations or a systematic error in age determination. Alternatively, assessing the potential distribution of ages from individual zoned grains (e.g. spot-dating with laser ablation ICP-MS and age modeling across zones) could quantify and predict potential systematic error (Boyce & Hodges, 2005). The difference between the fluvial and glacial curves, however, preserves some relevance since any systematic shift toward older ages would affect both PDFs equally.

Coupled erosion processes and implications for Teton landscape evolution

One goal of this application of detrital thermochronometry is to identify spatial patterns of erosion across different altitudinal domains of a basin. Results for Garnet Canyon show that over short glacial-interglacial cycles, this system is not in steady state, but relative similarities between glacial, fluvial and predicted PDFs may indicate the landscape is approaching spatially uniform erosion over longer scales, consistent with the interpretations of Foster *et al.* (2010). Although glaciers efficiently erode the valley floors of small catchments, they are not producing large cirques or overdeepenings observed in larger basins. Weathering and mass wasting along hillslopes must equal glacial valley incision in Garnet Canyon, such that basin topography evolves relatively little when viewed across climatic cycles. These processes are balanced such that despite the apparent difference in long-term erosion at peaks vs valleys below the Paleozoic unconformity, significant relief production is limited in smaller basins.

Results also provide insight into how individual erosion mechanisms interact to produce the rugged topography of this small basin. Alpine glaciers are highly efficient at modifying topography (Harbor & Warburton, 1993; Kirkbride & Matthews, 1997; Brocklehurst & Whipple, 2002; Montgomery, 2002), however, our results indicate limits to the glacial erosion system. The lack of focused erosion at low altitudes suggests that the recent valley glacier system is stable and adjusted to the size and conditions of this basin. Glacial incision was probably more important in shaping Garnet Canyon than fluvial incision over the long-term, but was recently limited. The apparent stability of glacial erosion in Garnet Canyon generally agrees with the assessments of Foster *et al.* (2010) that type II basins of the Teton Range are presently adjusted to the modern climatic conditions, whereas larger basins are not. This implies that the response of erosional efficiency and topography to climate change is scale dependent.

An interesting implication of the 'dynamic topographic steady-state' proposed by Foster *et al.* (2010) is that the mass efflux from a basin will be overwhelmingly dominated by sediment sourced from hillslopes rather than valley bottoms. In Garnet Canyon this is evident in the extensive talus deposits that armor the valley floor. We speculate that the apparent steady-state is actually achieved through a complex set of evolving process interactions related to transport of the vast quantities of sediment produced by hillslopes. Large talus aprons imply that the interglacial alpine fluvial system is locally transport-limited and unable to keep pace with mass wasting. During glacial periods, glacial erosion must remove colluvial sediment that accumulated during the interglacial period before valley incision. The repeated advances of glaciers in small catchments thus may be necessary as much for sediment transport as for canyon incision (Brocklehurst & Whipple, 2007). Thick talus fans deposited during interglacial periods may also enhance bedrock chemical weathering via trapped groundwater thereby facilitating periodic glacial incision or fluvial transport during peak flow conditions (Small *et al.*, 1999). Mid-sized and small basins only weakly modify topography, while larger valleys experience transient conditions due to the power of larger glacial systems.

Hillslopes must erode rapidly and consistently across glacial cycles to achieve steady-state topography in Garnet Canyon, which may be facilitated by earlier and continued glacial oversteepening. If little or no valley incision occurs during interglacial periods and hillslopes continue to denude rapidly, relief may decrease temporarily. Conditions enabling rapid mass wasting (frost cracking, pervasive fractures) may thus play an important role in shaping and limiting topography. The height of 'teflon peaks' that extend above the glacial buzzsaw, as proposed by Foster *et al.* (2010), may thus be controlled by a myriad of small-scale processes. Additional data on rock mass strength, hillslope denudation rates, and talus accumulation rates will better quantify the influence of these factors. Future work may further elucidate the controls on alpine topography by focusing on the conditions that affect individual erosional mechanisms and the feedback loops between them.

CONCLUSIONS

We have assessed the applicability of detrital AHe thermochronology for estimating the efficiency and spatial patterns of erosional processes at different altitudinal zones during a short-term change in climate conditions. Because dynamic interactions between erosional processes control development and relief of alpine basins, it is necessary to

investigate each process so as to obtain a comprehensive understanding of the entire landscape.

Detrital cooling ages from glacial and fluvial deposits in Garnet Canyon record some variable erosion patterns. Discordance from the predicted PDF is most evident in a pulse of old ages in both deposits, reflecting effective sediment routing in this small basin and suggesting that high elevations may be eroding more aggressively than predicted. This signal may alternatively be an artifact due to systematic age overestimation associated with poor sample quality or underestimating the maximum elevation age. Results show the fluvial system is transport limited at mid-altitudes, where glacial erosion is focused. This zone may be buried by hillslope talus that is only removed to allow bedrock erosion during glacial maxima. Remarkably, the distributions of the detrital cooling ages do not differ dramatically, despite extreme differences in erosional dynamics between the glacial and interglacial periods. Despite deep valleys, steep hillslopes, and basin-wide differences in long-term average incision rate below a Paleozoic unconformity, relief is not currently being produced and topography is approaching steady-state when averaged across glacial and interglacial periods. The glacier system is adjusted to this basin size and rapid incision is limited. We speculate that a myriad of interacting erosional processes are currently controlling basin relief and the height of 'teflon peaks.'

While this method records variations in the spatial pattern of erosional efficiency, its accuracy is highly dependent on the quality of detrital apatite grains and their suitability for AHe dating. Our results suggest that the assumption of uniform apatite yield may be invalid in geologically complex basins, given that subtle changes in lithology can coincide with order of magnitude changes in datable apatite yield. Both variation of bedrock relative to basin hypsometry and apatite quality should be assessed before detailed sampling and intense laboratory effort. As other studies have shown, our results indicate that the presence of micro-inclusions and compositional zonation are significant problems for AHe thermochronology. Sample characterization using SEM, CL, and other imaging techniques, as well as careful documentation of single grain age reproducibility and apatite yield in multiple bedrock samples should be performed in any detrital thermochronology study using AHe dating. The short-term spatial variations in erosion that we observed support conclusions by Ruhl & Hodges (2005) that assuming uniform erosion when estimating cooling history from single 'grab bag' samples may be risky. Despite the potential pitfalls, however, our results show that detrital AHe thermochronology is a useful tool for assessing erosional variability and geomorphic evolution of small basins.

SUPPORTING INFORMATION

Additional Supporting Information may be found in the online version of this article:

Fig. S1. Photos of detrital sample locations. (a) Sample TTS-1 was collected from a quickly flowing section of the Garnet Canyon stream, near the bank where sediments were able to settle (Fig. 5a). (b) Sample TTS-3 was collected on the innermost moraine ridge north of Bradley Lake after removal of the upper ~5 cm of material and vegetation debris from the surface (Fig. 5a). Observations of 100 clasts from this moraine showed that the vast majority (99%) was derived from the typical igneous and metamorphic rocks found in Garnet Canyon, and thus were not mixed with sediment pushed by large valley glaciers along the floor of Jackson Hole.

Fig. S2. Sampling distributions of Kuiper asymptotic statistic [Ka] estimated using Monte Carlo simulations. Each distribution is based on a separate simulation consisting of 1000 replicate samples drawn randomly from the probability function given by the PDF estimated with hypsometry and age-elevation relationship. Arrows indicate the value of Ka statistic for the actual sample. (a) A simulation for the fluvial dataset (sample size $n = 77$) for 10% uncertainty; (b) A simulation for the glacial dataset (sample size $n = 60$) for 10% uncertainty; (c) A simulation for the fluvial dataset (sample size $n = 77$) for 20% uncertainty; (d) A simulation for the glacial dataset (sample size $n = 60$) for 20% uncertainty. See Supplementary text and Table S3 for additional information.

Fig. S3. PDF calculated with 20% uncertainty for ages predicted with the age-elevation relationship excluding sample TT-1 (Equation: $y = 18.314 \times +2396$). The maximum predicted age is 98 Ma. The glacial distribution has fewer significant old ages, but the fluvial system still produces an abundance of old ages. Ages as old as 100 Ma are unexpected, however, based on apatite fission track studies in the area (Roberts & Burbank, 1993).

Table S1. AHe data for detrital grains.

Table S2. Kuiper statistic results.

Table S3. Statistical estimates of observed differences in shapes of age distributions derived using Monte Carlo simulations. The difference in shape of distributions measured using Kuiper asymptotic [Ka] statistic. See Monte Carlo methods for detailed explanation of the resampling protocol. Four separate 1000-iteration simulations are reported below.

Please note: Wiley-Blackwell is not responsible for the content or functionality of any supporting materials supplied by the authors. Any queries (other than missing material) should be directed to the corresponding author for the article.

REFERENCES

Amidon, W.H., Burbank, D.W. & Gehrels, G.E. (2005) Construction of detrital mineral populations: insights from mixing of U-Pb zircon ages in Himalayan rivers. *Basin Res.*, **17**, 463–485.

Anders, M.H. & Sleep, N.H. (1992) Magmatism and extension: the thermal and mechanical effects of the Yellowstone hotspot. *J. Geophys. Res.*, **97**, 15379–15393.

Anderson, R.S., Riihimaki, C.A., Safran, E.B. & MacGregor, K.R. (2006) Facing reality: late Cenozoic evolution of smooth peaks, glacially ornamented valleys, and deep river gorges of Colorado's Front Range. In: *Tectonics, Climate, and Landscape Evolution* (Ed. by S.D. Willett, N. Hovius, M.T. Brandon & D.M. Fisher), *Geol. Soc. Am. Spec. Pap. 398*. pp. 397–418. The Geological Society of America, Boulder, CO.

Arsenault, A.M. & Meigs, A.J. (2005) Contribution of deep-seated bedrock landslides to erosion of a glaciated basin in southern Alaska. *Earth Surface Process. Landforms*, **30**, 1111–1125.

Attal, M. & Lave, J. (2006) Changes of bedload characteristics along the Marsyandi River (central Nepal): implications for understanding hillslope sediment supply, sediment load evolution along fluvial networks, and denudation in active orogenic belts. In: *Tectonics, Climate, and Landscape Evolution* (Ed. by S.D. Willett, N. Hovius, M.T. Brandon & D.M. Fisher), *Geol. Soc. Am. Spec. Pap.*, **398**, 143–171.

Barnosky, A.D. (1984) The Colter Formation: evidence for Miocene volcanism in Jackson Hole, Teton County, Wyoming. *Wyoming Geol. Assoc. Earth Sci. Bull.*, **17**, 49–95.

Berger, A.L., Spotila, J.A., Chapman, J.B., Pavlis, T.L., Enkelmann, E., Ruppert, N.A. & Buscher, J.T. (2008) Architecture, kinematics, and exhumation of a convergent orogenic wedge: a thermochronological investigation of tectonic-climatic interactions within the central St. Elias orogen, Alaska. *Earth Planetary Sci. Lett.*, **270**, 13–24.

Boyce, J.W. & Hodges, K.V. (2005) U and Th zoning in Cerro de Mercado (Durango, Mexico) fluorapatite: insights regarding the impact of recoil redistribution of radiogenic ^{4}He on (U-Th)/He thermochronology. *Chem. Geol.*, **219**, 261–274.

Bradley, C.C. (1956) The pre-Cambrian complex of Grand Teton National Park, Wyoming: Wyoming Geological Association Guidebook, 11th Annual Field Conference.

Brewer, I.D. & Burbank, D.W. (2006) Thermal and kinematic modeling of bedrock and detrital cooling ages in the central Himalaya. *J. Geophys. Res.*, **111**, B09409.

Brewer, I.D., Burbank, D.W. & Hodges, K.V. (2003) Modelling detrital cooling-age populations: insights from two Himalayan catchments. *Basin Res.*, **15**, 305–320.

Brewer, I.D., Burbank, D.W. & Hodges, K.V. (2006) Downstream development of a detrital cooling-age signal: Insights from ^{40}Ar/^{39}Ar muscovite thermochronology in the Nepalese Himalaya. In: *Tectonics, Climate, and Landscape Evolution* (Ed. by S.D. Willett, N. Hovius, M.T. Brandon & D.M. Fisher), *Geol. Soc. Am. Spec. Pap. 398*. pp. 321–338. The Geological Society of America, Boulder, CO.

Brocklehurst, S. & Whipple, K.X. (2007) Response of glacial landscapes to spatial variations in rock uplift rate. *J. Geophys. Res.*, **112**, F02035.

Brocklehurst, S.H. & Whipple, K.X. (2002) Glacial erosion and relief production in the Eastern Sierra Nevada, California. *Geomorphology*, **42**, 1–24.

Brocklehurst, S.H. & Whipple, K.X. (2004) Hypsometry of glaciated landscapes. *Earth Surface Process. Landforms*, **29**, 907–926.

Brown, S.J. (2010) Integrating apatite (U-Th)/He and fission-track dating for a comprehensive thermochronological analysis: refining the uplift history of the Teton Range. Master's thesis, Blacksburg, VA, Virginia Tech.

Brozovic, N., Burbank, D.W. & Meigs, A.J. (1997) Climatic limits on landscape development in the Northwestern Himalaya. *Science*, **276**, 571–574.

Burbank, D.W., Leland, J., Fielding, E., Anderson, R.S., Brozovic, N., Reid, M.R. & Duncan, C. (1996) Bedrock incision, rock uplift and threshold hillslopes in the northwestern Himalayas. *Nature*, **379**, 505–510.

Buscher, J.T. & Spotila, J.A. (2007) Near-field response to transpression along the southern San Andreas fault, based on exhumation of the northern San Gabriel Mountains, southern California. *Tectonics*, **26**, TC5004.

Byrd, J.O.D. (1995) Neotectonics of the Teton Fault, Wyoming. Doctoral thesis, Salt Lake City, UT, University of Utah.

Carrapa, B. & Strecker, M.R. (2005) The sedimentary record of intramontane basins in the southern Central Andes; insight into tectonic versus surface processes interactions in the creation of the Puna Plateau, Abstracts with Programs – Geological Society of America. Vol. 37, Salt Lake City, UT, 481.

Cawood, P.A., Nemchin, A.A., Freeman, M. & Sircombe, K. (2003) Linking source and sedimentary basin: detrital zircon record of sediment flux along a modern river system and implications for provenance studies. *Earth Planet. Sci. Lett.*, **210**, 259–268.

Cawood, P.A., Nemchin, A.A. & Strachan, R. (2007) Provenance record of Laurentian passive-margin strata in the northern Caledonides: implications for paleodrainage and paleogeography. *Geol. Soc. Am. Bull.*, **119**, 993–1003.

Cerveny, P.F., Naeser, N.D., Zeitler, P.K., Naeser, C.W. & Johnson, N.M. (1988) History of uplift and relief of the Himalaya during the past 18 million years; evidence from fission-track ages of detrital zircons from sandstones of the Siwalik Group. In: *New Perspectives in Basin Analysis: Frontiers in Sedimentary Petrology* (Ed. by K.L. Kleinspehn & C. Paola), pp. 43–61. Springer-Verlag, New York, NY.

Corrigan, J.D. & Crowley, K.D. (1992) Unroofing of the Himalayas: a view from apatite fission-track analysis of Bengal Fan sediments. *Geophys. Res. Lett.*, **19**, 2345–2348.

Duhnforth, M., Densmore, A.L., Ivy-Ochs, S. & Allen, P.A. (2008) Controls on sediment evacuation from glacially modified and unmodified catchments in the eastern Sierra Nevada, California. *Earth Surface Process. Landforms*, **33**, 1602–1613.

Ehlers, T.A. & Farley, K.A. (2003) Apatite (U-Th)/He thermochronometry: methods and applications to problems in tectonic and surface processes. *Earth Planet. Sci. Lett.*, **206**, 1–14.

Emmel, B., Jacobs, J., Crowhurst, P. & Daszinnies, M.C. (2007) Combined apatite fission-track and single grain apatite (U-Th)/He ages from basement rocks of central Dronning Maud Land (East Antarctica) - Possible identification of thermally overprinted crustal segments. *Earth Planet. Sci. Lett.*, **264**, 72–88.

Emmel, B., Jacobs, J., Crowhurst, P.V., Austegard, A. & Schwarz-Schampera, U. (2008) Apatite single-grain (U-Th)/He data from Heimefrontfjella, East Antarctica: indications for exhumation related to glacial loading? *Tectonics*, **27**, TC6010.

Farley, K.A. (2000) Helium diffusion from apatite: general behavior as illustrated by Durango fluorapatite. *J. Geophys. Res.*, **105**, 2903–2914.

Farley, K.A. & Stockli, D.F. (2002) (U-Th)/He dating of phosphates; apatite, monazite, and xenotime. In: *Reviews in Mineralogy and Geochemistry*, **Vol. 48** (Ed. by M.J. Kohn, J. Rakovan & J.M. Hughes), pp. 559–577. Mineralogical Society of America and Geochemical Society, Washington, DC.

Farley, K.A., Wolf, R.A. & Silver, L.T. (1996) The effects of long alpha-stopping distances on (U-Th)/He ages. *Geochim. Cosmochim. Acta*, **60**, 4223–4229.

Fedo, C.M., Sircombe, K.N. & Rainbird, R.H. (2003) Detrital Zircon Analysis of the Sedimentary Record. In: *Reviews in Mineralogy & Geochemistry* (Ed. by J.M. Hanchar & P.W.O. Hoskin). **53**, 277–303.

Fitzgerald, P.G., Baldwin, S.L., Webb, L.E. & O'Sullivan, P.B. (2006) Interpretation of (U-Th)/He single grain ages from slowly cooled crustal terranes: a case study from the Transantarctic Mountains of southern Victoria Land. *Chem. Geol.*, **225**, 91–120.

Flowers, R.M. (2009) Exploiting radiation damage control on apatite (U-Th)/He dates in cratonic regions. *Earth Planet. Sci. Lett.*, **277**, 148–155.

Flowers, R.M., Ketcham, R.A., Shuster, D.L. & Farley, K.A. (2009) Apatite (U-Th)/He thermochronometry using a radiation damage accumulation and annealing model. *Geochim. Cosmochim. Acta*, **73**, 2347–2365.

Foster, D., Brocklehurst, S.H. & Gawthorpe, R.L. (2008) Small valley glaciers and the effectiveness of the glacial buzzsaw in the northern Basin and Range, USA. *Geomorphology*, **102**, 624–639.

Foster, D., Brocklehurst, S.H. & Gawthorpe, R.L. (2010) Glacial-topographic interactions in the Teton Range, Wyoming. *J. Geophys. Res.*, **115**, F01007.

Frost, R., Frost, C.D., Cornia, M., Chamberlain, K.R. & Kirkwood, R. (2006) The Teton-Wind River domain: a 2.68–2.67 Ga active margin in the western Wyoming Province. *Canad. J. Earth Sci.*, **43**, 1489–1510.

Garver, J.I., Brandon, M.T., Roden-Tice, M.K. & Kamp, P.J.J. (1999) Exhumation history of orogenic highlands determined by detrital fission-track thermochronology. *Geol. Soc. Spec. Publ.*, **154**, 283–304.

Green, P.F., Crowhurst, P.V., Duddy, I.R., Jaspen, P. & Holford, S.P. (2006) Conflicting (U-Th)/He and fission track ages in apatite; enhanced He retention, not anomalous annealing behaviour. *Earth Planet. Sci. Lett.*, **250**, 407–427.

Haeussler, P.J., O'Sullivan, P., Berger, A.L. & Spotila, J.A. (2008) Neogene exhumation of the Tordrillo Mountains, Alaska, and correlations with Denali (Mount McKinley). In: *Active Tectonics and Seismic Potential of Alaska*, **Vol. 179** (Ed. by J.T. Freymueller, P.J. Haeussler, R.L. Wesson & G. Ekstrom), pp. 269–285. American Geophysical Union, Washington, DC.

Hales, T.C. & Roering, J.J. (2007) Climatic controls on frost cracking and implications for the evolution of bedrock landscapes. *J. Geophys. Res.*, **112**, F02033.

Hampel, A., Hetzel, R. & Densmore, A.L. (2007) Postglacial slip-rate increase on the Teton normal fault, northern Basin and Range Province, caused by melting of the Yellowstone ice cap and deglaciation of the Teton Range? *Geology*, **35**, 1107–1110.

Harbor, J.M. (1992) Numerical modeling of the development of U-shaped valleys by glacial erosion. *Geol. Soc. Am. Bull.*, **104**, 1364–1375.

Harbor, J.M. & Warburton, J. (1993) Relative rates of glacial and nonglacial erosion in alpine environments. *Arctic Alpine Res.*, **25**, 1–7.

Harkins, N., Kirby, E., Heimsath, A., Robinson, R. & Reiser, U. (2007) Transient fluvial incision in the headwaters of the Yellow River, northeastern Tibet, China. *J. Geophys. Res.*, **112**, F03S04.

House, M.A., Wernicke, B.P., Farley, K.A. & Dumitru, T.A. (1997) Cenozoic thermal evolution of the central Sierra Nevada, California, from (U-Th)/He thermochonometry. *Earth Planet. Sci. Lett.*, **151**, 167–179.

Jolivet, M., Dempster, T.J. & Cox, R. (2003) Distribution of U and Th in apatites: implications for U-Th/He thermochronology: Comptes Rendus – Academie des Sciences. *Geoscience*, **335**, 899–906.

Kirkbride, M. & Matthews, D. (1997) The role of fluvial and glacial erosion in landscape evolution: the Ben Ohau Range, New Zealand. *Earth Surface Process. Landforms*, **22**, 317–327.

Korup, O. & Schlunegger, F. (2007) Bedrock landsliding, river incision, and transcience of gemorphic hillslope-channel coupling: evidence from inner gorges in the Swiss Alps. *J. Geophys. Res.*, **112**, F03027.

Kowalewski, M. & Rimstidt, J.D. (2003) Average lifetime and age spectra of detrital grains: toward a unifying theory of sedimentary particles. *J. Geol.*, **111**, 427–439.

Kuiper, N.H. (1960) Tests concerning random points on a circle. *Proc. Koninklijke Nederlandse Akad.van Wetenschappen*, **63**, 38–47.

Leopold, E.B., Liu, G., Love, J.D. & Love, D.W. (2007) Plio-Pleistocene climate transition and the lifting of the Teton Range, Wyoming. *Quat. Res.*, **67**, 1–11.

Li, Y., Harbor, J.M., Stroeven, A.P., Fabel, D., Kleman, J., Fink, D., Caffee, M. & Elmore, D. (2005) Ice sheet erosion patterns in valley systems in northern Sweden investigated using cosmogenic nuclides. *Earth Surface Process. Landforms*, **30**, 1039–1049.

Licciardi, J.M. & Pierce, K.L. (2008) Cosmogenic exposure-age chronologies of Pinedale and Bull Lake glaciations in greater Yellowstone and the Teton Range, USA. *Quat. Sci. Rev.*, **27**, 814–831.

Love, J.D. (1977) Summary of Upper Cretaceous and Cenozoic stratigraphy and of tectonic and glacial events in Jackson Hole, northwestern Wyoming: Wyoming Geological Association Guidebook, 29th Annual Field Conference Guidebook, pp. 585–593.

Love, J.D., Reed, J.C. Jr. & Christiansen, A.C. (1992) Geologic Map of Grand Teton National Park, Teton County, Wyoming, Map I-2031. Scale 1:62500. U.S. Geological Survey, Reston, VA.

Love, J.D., Reed, J.C. Jr. & Pierce, K.L. (2003) *Creation of the Teton Landscape*. Grand Teton Natural History Association, Moose, Wyoming, 132pp.

Machette, M.N., Pierce, K.L., McCalpin, J.P., Haller, K.M. & Dart, R.L. (2001) *Map and Data for Quaternary Faults and Folds in Wyoming*. Open file report. U.S. Geological Survey, Reston, VA, 158pp.

McAleer, R.J., Spotila, J.A., Enkelmann, E. & Berger, A.L. (2009) Exhumation along the Fairweather fault, southeastern Alaska, based on low-temperature thermochronometry. *Tectonics*, **28**, TC1007.

McDowell, F.W., McIntosh, W.C. & Farley, K.A. (2005) A precise ^{40}Ar-^{39}Ar reference age for the Durango apatite (U-Th)/He and fission-track dating standard. *Chem. Geol.*, **214**, 249–263.

Meesters, A.G.C.A. & Dunai, T.J. (2002) Solving the production-diffusion equation for finite diffusion domains of various shapes. Part I. Implications for low-temperature (U-Th)/He thermochronology. *Chem. Geol.*, **186**, 333–344.

Mitchell, S.G. & Montgomery, D.R. (2006) Influence of a glacial buzzsaw on the height and morphology of the Cascade Range in central Washington State, USA. *Quat. Res.*, **65**, 96–107.

Mitchell, S.G. & Reiners, P.W. (2003) Influence of wildfires on apatite and zircon (U-Th)/He ages. *Geology*, **31**, 1025–1028.

Montgomery, D.R. (2002) Valley formation by fluvial and glacial erosion. *Geology*, **30**, 1047–1050.

Oskin, M.E. & Burbank, D. (2007) Transient landscape evolution of basement-cored uplifts: example of the Kyrgyz Range, Tian Shan. *J. Geophys. Res.*, **112**, F03S03.

Ouimet, W.B., Whipple, K.X. & Granger, D.E. (2009) Beyond threshold hillslopes: channel adjustment to base-level fall in tectonically active mountain ranges. *Geology*, **37**, 579–582.

Pierce, K.L. & Morgan, L.A. (1992) The track of the Yellowstone hot spot; volcanism, faulting, and uplift. In: *Regional Geology of Eastern Idaho and Western Wyoming* (Ed. by P.K. Link, M.A. Kuntz & L.B. Platt), *Geol. Soc. Am. Mem.*, **179**, 1–53.

Porter, S.C., Pierce, K.L. & Hamilton, T.D. (1983) Late Wisconsin mountain glaciation in the Western United States. In: *The Late Pleistocene* (Ed. by S.C. Porter), pp. 71–111. University of Minnesota Press, Minneapolis, MN.

Puskas, C.M. & Smith, R.B. (2009) Intraplate deformation and microplate tectonics of the Yellowstone hot spot and surrounding western U.S. interior. *J. Geophys. Res.*, **114**, B04410.

Rahl, J.M., Ehlers, T.A. & van der Pluijm, B.A. (2007) Quantifying transient erosion of orogens with detrital thermochronology from syntectonic basin deposits. *Earth Planetary Sci. Lett.*, **256**, 147–161.

Rahl, J.M., Reiners, P.W., Campbell, I.H., Nicolescu, S. & Allen, C.M. (2003) Combined single-grain (U-Th)/He and U/Pb dating of detrital zircons from the Navajo Sandstone, Utah. *Geology*, **31**, 761–764.

Reed, J.C.J. & Zartman, R.E. (1973) Geochronology of Precambrian Rocks of the Teton Range, Wyoming. *Geol. Soc. Am. Bull.*, **84**, 561–582.

Reiners, P.W. & Farley, K.A. (2001) Influence of crystal size on apatite (U-Th)/He thermochronology: an example from the Bighorn Mountains, Wyoming. *Earth Planetary Sci. Lett.*, **188**, 413–420.

Reiners, P.W., Thomson, S.N., McPhillips, D., Donelick, R.A. & Roering, J.J. (2007) Wildfire thermochronology and the fate and transport of apatite in hillslope and fluvial environments. *J. Geophys. Res.*, **112**, F04001.

Riihimaki, C.A., Anderson, R.S. & Safran, E.B. (2007) Impact of rock uplift on rates of late Cenozoic Rocky Mountain river incision. *J. Geophys. Res.*, **112**, F03S02.

Roberts, S.V. & Burbank, D.W. (1993) Uplift and thermal history of the Teton Range (northwestern Wyoming) defined by apatite fission-track dating. *Earth Planetary Sci. Lett.*, **118**, 295–309.

Ruhl, K.W. & Hodges, K.V. (2005) The use of detrital mineral cooling ages to evaluate steady state assumptions in active orogens: an example from the central Nepalese Himalaya. *Tectonics*, **24**, TC4015.

Schmidt, K.M. & Montgomery, D.R. (1995) Limits to Relief. *Science*, **270**, 617–620.

Shuster, D.L. & Farley, K.A. (2009) The influence of artificial radiation damage and thermal annealing on helium diffusion kinetics in apatite. *Geochim. Cosmochim. Acta*, **73**, 183–196.

Small, E.E. & Anderson, R.S. (1998) Pleistocene relief production in Laramide mountain ranges, western United States. *Geology*, **26**, 123–126.

Small, E.E., Anderson, R.S. & Hancock, G.S. (1999) Estimates of the rate of regolith production using ^{10}Be and ^{26}Al from an alpine hillslope. *Geomorphology*, **27**, 131–150.

Smith, R.B., Byrd, J.O.D. & Susong, D.D. (1993) The Teton Fault, Wyoming: Seismotectonics, Quaternary History, and Earthquake Hazards. In: *Geology of Wyoming* (Ed. by A.W. Snoke, J.R. Steiatmann & S.M. Roberts), **Vol. 5**, 628–667. Geological Survey of Wyoming, Laramie, WY.

Spotila, J.A., Bank, G.C., Reiners, P.W., Naeser, C.W., Naeser, N.D. & Henika, B.S. (2004) Origin of the Blue Ridge escarpment along the passive margin of Eastern North America. *Basin Res.*, **16**, 41–63.

Stephens, M.A. (1965) The goodness-of-fit statistic V_N: distribution and significance points. *Biometrika*, **52**, 309–321.

Stock, G.M., Ehlers, T.A. & Farley, K.A. (2006) Where does sediment come from? Quantifying catchment erosion with detrital apatite (U-Th)/He thermochronometry. *Geology*, **34**, 725–728.

Stock, J.D. & Montgomery, D.R. (1996) Estimating Paleorelief from detrital mineral age ranges. *Basin Research*, **8**, 317–327.

Straumann, R.K. & Korup, O. (2009) Quantifying postglacial sediment storage at the mountain-belt scale. *Geology*, **37**, 1079–1082.

Vermeesch, P. (2004) How many grains are needed for a provenance study? *Earth Planetary Sci. Lett.*, **224**, 441–451.

Vermeesch, P. (2007) Quantitative geomorphology of the White Mountains (California) using detrital apatite fission track thermochronology. *J. Geophys. Res.*, **112**, F03004.

Whipp, D.M.J., Ehlers, T.A., Braun, J. & Spath, C.D. (2009) Effects of exhumation kinematics and topographic evolution on detrital thermochronometer data. *J. Geophysi. Res.*, **114**, F04021.

Whipple, K.X., Kirby, E. & Brocklehurst, S.H. (1999) Geomorphic limits to climate-induced increases in topographic relief. *Nature*, **401**, 39–43.

Willett, S.D. & Brandon, M.T. (2002) On steady states in mountain belts. *Geology*, **30**, 175–178.

Wolf, R.A., Farley, K.A. & Silver, L.T. (1996) Helium diffusion and low-temperature thermochronometry of apatite. *Geochim. Cosmochim. Acta*, **60**, 4231–4140.

Zartman, R.E. & Reed, J.C. Jr. (1998) Zircon geochronology of the Webb Canyon Gneiss and Mount Owen Quartz Monzonite, Teton Range, Wyoming: significance to dating late Archean metamorphism in the Wyoming Craton. *Mounain Geol.*, **35**, 71–77.

Manuscript received 5 May 2010; In revised form 23 September 2010; Manuscript accepted 16 December 2010.